Article

Analyses and Simulations of PM$_{2.5}$ Pollution Characteristics under the Influence of the New Year's Day Effects in China

Qiao Shi [1], Tangyan Hou [1], Chengli Wang [2], Zhe Song [1], Ningning Yao [3], Yuhai Sun [3], Boqiong Jiang [3], Pengfei Li [4,*], Zhibin Wang [1] and Shaocai Yu [3,*]

[1] Key Laboratory of Environmental Remediation and Ecological Health, Ministry of Education, Research Center for Air Pollution and Health, College of Environmental and Resource Sciences, Zhejiang University, Hangzhou 310058, China; 22114078@zju.edu.cn (Q.S.); houtangyan@zju.edu.cn (T.H.); song_zhe@zju.edu.cn (Z.S.); wangzhibin@zju.edu.cn (Z.W.)

[2] Liaocheng Xinyuan Group Co., Ltd., Liaocheng 252000, China; hywangchengli@163.com

[3] School of Environmental Sciences and Engineering, Zhejiang Gongshang University, Hangzhou 310018, China; 23010040033@pop.zjgsu.edu.cn (N.Y.); yhsun@zjgsu.edu.cn (Y.S.); jiangboqiong@zjgsu.edu.cn (B.J.)

[4] State Key Laboratory of Infrared Physics, Shanghai Institute of Technical Physics, Chinese Academy of Sciences, Shanghai 200031, China

* Correspondence: pengfeili@mail.sitp.ac.cn (P.L.); shaocaiyu@zjgsu.edu.cn (S.Y.)

Abstract: Regional haze often occurs after the New Year holiday. To explore the characteristics of PM$_{2.5}$ pollutions under the influence of the New Year's Day effect, this study analyzed the spatiotemporal changes relating to PM$_{2.5}$ during and around the New Year's Day holiday in China from 2015 to 2022, and used the Weather Research and Forecasting-Community Multiscale Air Quality (WRF-CMAQ) model to study the effects of human activities and meteorological factors on PM$_{2.5}$ pollutions, as well as the differences in the contributions of different industries to PM$_{2.5}$ pollutions. The results show that for the entire study period (i.e., before, during, and after the New Year's Day holiday) from 2015 to 2022, the average concentrations of PM$_{2.5}$ in China decreased by 41.9% overall. In 2019~2022, the New Year's Day effect was significant, meaning that the average concentrations of PM$_{2.5}$ increased by 18.9~46.8 $\mu g/m^3$ from before to after the New Year's Day holiday, with its peak occurring (64.3~74.9 $\mu g/m^3$) after the holiday. In terms of spatial differences, the average concentrations of PM$_{2.5}$ were higher in the Beijing–Tianjin–Hebei region, the Yangtze River Delta, and central China. Moreover, the Beijing–Tianjin–Hebei region and its surrounding areas, the Chengdu–Chongqing region, the Fenwei Plain, and the middle reaches of the Yangtze River region were greatly affected by the New Year's Day effect. Human activities led to higher increases in PM$_{2.5}$ in Henan, Hubei, Hebei, and Anhui on 3 and 4 January 2022. If the haze was accompanied by cloudy days or weak precipitation, the accumulation of surface water vapor and atmospheric aerosols further increased the possibility of heavy pollution. It was found that, for the entire study period, PM$_{2.5}$ generated by residential sources contributed the vast majority (60~100 $\mu g/m^3$) of PM$_{2.5}$ concentrations, and that the main industry sources that caused changes in time distributions were industrial and transportation sources.

Keywords: WRF-CMAQ; New Year's Day effect; PM$_{2.5}$; smog; spatiotemporal variation

1. Introduction

Since the winter of 2013, China has repeatedly experienced severe regional air pollution. During the formation, evolution, and migration of haze, fine particulate matter (PM$_{2.5}$) with an aerodynamic diameter $\leq$ 2.5 μm plays a crucial role [1]. According to the formation processes of PM$_{2.5}$, it can be divided into primary PM, which is directly discharged into the atmosphere, and secondary PM, which is produced by the chemical transformation of gaseous pollutants [2–5]. Primary PM mainly comes from the combustion

of plants and mineral fuels, as well as dust particles [6]. Secondary PM mainly comes from aerosols generated by a series of chemical reactions of volatile organic compounds (VOCs), NO_x, and SO_2 in the atmosphere [7]. Studies have shown that $PM_{2.5}$, due to its small particle size and large specific surface area, is more prone to enrichment with heavy metals, oxides, and organic pollutants in the air. It can be transported over long distances and stays in the atmosphere for a long time, thereby reducing atmospheric visibility and having serious impacts on human health and crops [8,9]. After being inhaled by the human body, $PM_{2.5}$ first penetrates into the gas exchange zone of the lungs [10], then enters the circulatory system through the respiratory barrier, and finally spreads throughout the body [11,12]. This not only leads to the increase in cardiorespiratory incidence rates and mortality [13–15], but also leads to the occurrence and development of diabetes and adverse birth outcomes [16–18]. What is even more concerning is that, even if the $PM_{2.5}$ level is far below the national standard, $PM_{2.5}$ still poses a significant risk to public health [19–21].

$PM_{2.5}$ exhibits different characteristics in terms of its spatiotemporal distributions. On a temporal scale, the seasonal and monthly variations in urban $PM_{2.5}$ concentrations exhibit a U-shaped pattern [22–24]. Dai et al. [25] studied the temporal variations in $PM_{2.5}$ concentrations in five mega cities: Hefei, Shanghai, Wuhan, Nanjing, and Hangzhou. They found that $PM_{2.5}$ concentrations were highest in winter and lowest in summer. There were also seasonal variations in $PM_{2.5}$ concentrations among the five cities, which might be related to differences in the population, size, and meteorological conditions of the cities. Song et al. [26] pointed out that the daily variations in $PM_{2.5}$ showed a bimodal pattern, with peaks occurring during the morning and evening. On the spatial scale, since the Chinese government took a series of actions to control air pollution in 2013, the levels of $PM_{2.5}$ have dropped significantly. For example, the Pearl River Delta and the Yangtze River Delta have improved significantly, and the most polluted area is still the North China Plain [27]. From 2015 to 2018, there was a clear but gradual shift in the average center of $PM_{2.5}$ concentrations from northeast to southwest [28]. In addition, some energy cities (such as cities in Shanxi Province), densely populated and economically developed mega cities (such as Beijing), and heavy industrial cities (such as cities in Hebei Province) still have high levels of $PM_{2.5}$ emissions [29]. In contrast, due to lower levels of dependence on the coal industries and favorable meteorological conditions for atmospheric diffusion and dilution, the $PM_{2.5}$ concentrations in southern China remain relatively low.

At the same time, some scholars have also conducted studies on the spatiotemporal changes in pollutant concentrations caused by the Spring Festival effect. For example, Deng et al. [30] studied the spatiotemporal variation characteristics of and reasons behind the Spring Festival effect as regards atmospheric pollutants in 31 cities in China during the Spring Festival period. They found that levels of $PM_{2.5}$ and SO_2 in cities were greatly affected by the fireworks and firecrackers set off on New Year's Eve (66% and 58% of affected cities, respectively), and that the concentrations of atmospheric pollutants in southern cities differed more in the middle and early stages of the Spring Festival than in northern cities. Chang et al. [31] analyzed the impact of the Spring Festival effect on air quality in the Chang–Zhu–Tan Metropolitan Area and found that the $PM_{2.5}$ concentration in the area after the Spring Festival (7 days) was 41.5% lower than during the Spring Festival period, indicating a significant post-holiday effect. However, there is relatively little research on the spatiotemporal changes caused by the New Year's Day effect. Zhou et al. [32] conducted an analysis of the characteristics of $PM_{2.5}$ pollutions in Shijiazhuang city before and after New Year's Day in 2019. Their results showed that the main components of $PM_{2.5}$ were secondary inorganic ions (65.4%), which mainly came from coal (24.4%) and industrial process sources (23.7%).

Therefore, it is necessary to study the spatiotemporal variation characteristics of and reasons behind the New Year's Day effect in China. This study analyzed the spatiotemporal variation characteristics of $PM_{2.5}$ during and around New Year's Day from 2015 to 2022 in China based on observational data, and used numerical simulation methods to analyze and explain the causes of $PM_{2.5}$ pollution during and around New Year's Day in 2022. The

WRF-CMAQ model was used for numerical simulations in this study. The WRF (Weather Research and Forecasting) model was jointly developed by multiple institutions, including the National Center for Atmospheric Research (NCAR) and the National Center for Environmental Prediction (NCEP) in the United States [33]. As a new generation of mesoscale numerical weather forecasting system, the WRF model is mainly applied in atmospheric research and operational forecasting [34]. Studies have shown that the ability of the WRF model used to simulate and forecast weather conditions can be improved by optimizing appropriate parameters in the study's areas [35,36]. CMAQ (Community Multiscale Air Quality) is a chemical transport model released by the United States Environmental Protection Agency (EPA, https://www.epa.gov/cmaq, accessed on 5 March 2024). It integrates information from multiple aspects such as emission inventories, meteorological conditions, and chemical mechanisms [37]. The WRF-CMAQ model is widely used to study the formation, migration and transformation, and spatiotemporal distribution characteristics of air pollutants [38]. Zhang et al. [39] used the WRF-CAMQ model to determine the reasons for the decreases in $PM_{2.5}$ concentrations in the "2 + 26" cities in the Beijing–Tianjin–Hebei (BTH) region during the 2017/18 heating season. They found that the contributions of emission reduction ranged from 2.3% to 81.6%, but that favorable meteorological conditions also played an important role. It has been proven that, under favorable meteorological conditions, implementing emission reduction measures in a combined manner was very conducive to improving air quality. Jiang et al. [40] used the WRF-CMAQ model to quantify the contribution of emission reduction measures and meteorological conditions to air quality improvement during the 2022 Beijing Winter Olympics. The results show that, under the scenarios of emission reduction measures and no emission reduction measures, favorable meteorological conditions in 2022 led to decreases of 6.9 and 11.8 $\mu g/m^3$ in $PM_{2.5}$ in Beijing, respectively. In addition, local emissions reductions contributed further to the good air quality in Beijing. A large number of this study's results have shown that the model has excellent performance in the field of atmospheric pollutant simulation [41–46]. Therefore, the WRF-CMAQ model is used to simulate $PM_{2.5}$ concentrations during and around the New Year's Day holiday in this study. This study's results provide a scientific basis for the rational evaluation of the effectiveness of air pollution prevention and control work, and the exploration of effective strategies for the joint prevents and control of air pollution.

2. Materials and Methods

2.1. Observational Data

The hourly concentration data of $PM_{2.5}$ pollutants, taken from 2025 monitoring stations nationwide (as of 2022), were downloaded from the National Environmental Monitoring Center (CNEMC) of China (http://www.cnemc.cn/, accessed on 6 April 2024). The hourly measured values of meteorological parameters (temperature (T), relative humidity (RH), wind speed (WS), and wind direction (WD)) were taken from the National Climate Data Center (NCDC) in the United States (ftp://ftp.ncdc.noaa.gov/pub/data/noaa/, accessed on 6 April 2024). The surface weather charts were provided by Hong Kong Observatory (http://envf.ust.hk/dataview/hko_wc/current/, accessed on 6 April 2024). This study used the above data to conduct a nationwide analysis of pollutant characteristics during and around the New Year's Day holiday from 2015 to 2022, and evaluated the simulation performances of the model. This research focused on nine regions [47] (Figure 1a, and compared the spatiotemporal changes seen in different regions. The entire period of time studied (i.e., before, during, and after the New Year's Day holiday) was divided into three periods: BNY: (two days) before the New Year's Day holiday; DNY: (three days (or one day)) during the New Year's Day holiday; and ANY: (two days) after the New Year's Day holiday.
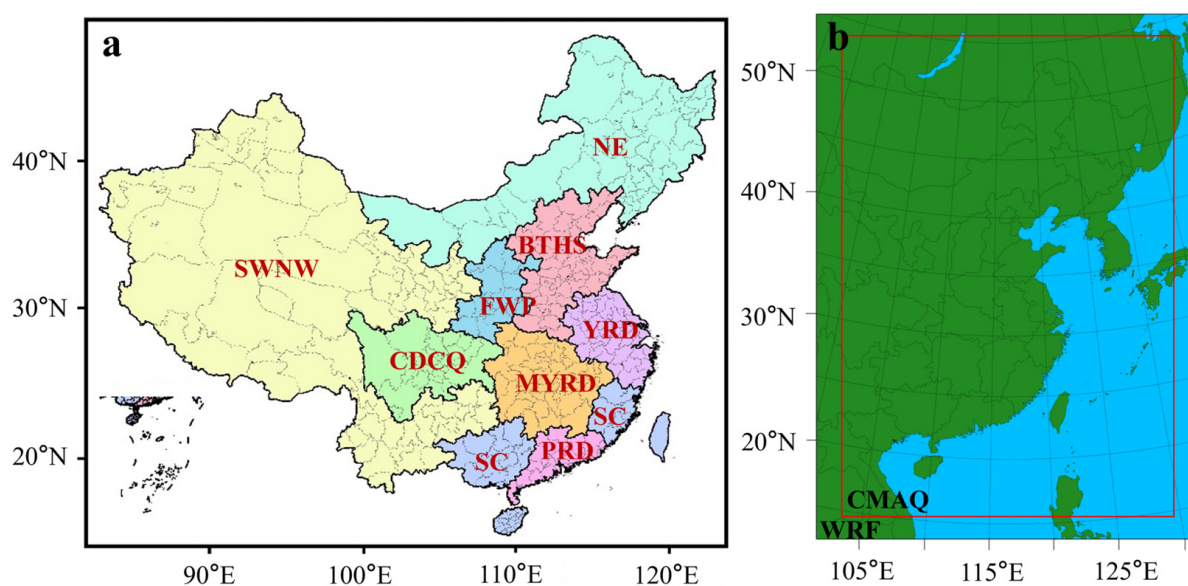
Figure 1. (**a**) Classification of study areas represented by different colors. Beijing–Tianjin–Hebei region and its surrounding areas (BTHS), Yangtze River Delta region (YRD), Fenwei Plain (FWP), Chengdu–Chongqing region (CDCQ), middle reaches of the Yangtze River region (MYRD), Pearl River Delta region (PRD), Northeast region (NE), Southern Coastal region (SC), and Southwest and Northwest region (SWNW). (**b**) The simulation area of the model, with the outermost layer being the simulation area of WRF and the CMAQ simulation area within the red box.

2.2. Model Configuration

The Weather Research and Forecasting-Community Multiscale Air Quality (WRF-CMAQ) model is widely used in air pollution studies [48–52]. In this study, a one-way coupled WRF (v4.0)-CMAQ (v5.0.2) model was adopted. In this model, the output of WRF mode was first converted into the format required by CMAQ using MCIP (Meteorology-Chemistry Interface Processor), and these data were then input in CMAQ mode. MCIP used version 5.0, which was a module set in CMAQ mode. The type and combination of physical parameterization used in the model determined whether the WRF model was suitable for specific research. Therefore, it is necessary to adjust the model's parameters for specific situations in the atmosphere [53]. However, this paper referred to the physical parameterization schemes selected in previous studies [39,40,54–56], which had been proven to be applicable to China and demonstrated good simulation performances when combined with CMAQ. The detailed physical parameterizations and chemical options in the WRF-CMAQ model were the same as those seen in Yu et al. [57]. In the vertical direction, WRFv4.0 used sigma coordinates with 29 layers, where the boundary layer (PBL) included about 10 layers. The maximum pressure of the WRF mode was fixed at 100 hPa. The PX (Pleim–Xiu) land surface scheme [58,59], te ACM2 (Asymmetric Convective Model version 2) boundary layer scheme [60,61], the Morrison double-moment cloud microphysics scheme [62,63], and the Kain–Fritsch 2 cumulus scheme were selected [64]. The RRTMG scheme was chosen for long- and short-wave radiation.

The FNL (Final Operational Global Analysis) meteorological field was applied to provide boundary and initial conditions for the WRF meteorological model. The FNL data were obtained from the National Centers for Environmental Prediction (NCEP) in the United States (https://rda.ucar.edu/datasets/ds083.2/dataaccess/#, accessed on 23 March 2024). The spatial resolution of the FNL data was $1° × 1°$, and the temporal resolution was 6 h.

The CMAQv5.0.2 version is consistent with the WRF mode in the vertical direction, as both have 29 layers. In terms of a calculation module, the CB05 meteorological chemical mechanism and AER06 aerosol module were adopted [37]. These two modules simultaneously considered gas-phase and liquid-phase chemical processes, the dry and wet deposition of pollutants, convection, and turbulence effects. The default initial and boundary chemical conditions provided in CMAQ were used. The simulation period was from 24 December 2021 to 5 January 2022. In order to reduce the impacts of initial chemical conditions on the simulation's results, the results of the first 4 days were discarded as model spin-up time.

Anthropogenic emission data were taken from the Multi-resolution Emission Inventory for China (MEIC) (http://www.meicmodel.org, accessed on 23 March 2024), developed by Tsinghua University, with a horizontal resolution of $0.25° \times 0.25°$. In the following part, Case16 and Case17 represented the simulated values with respect to the 2016 and 2017 emission inventories, respectively. Biological emissions data were taken from natural gas and aerosol emission models (MEGAN v2.1) [6,65]. The Biogenic Emission Inventory System version 3.14 (BEISv3.14) was used to calculate the natural sources of biological emission [56,57]. The ISAM (Integrated Source Apportionment Method) source apportionment tool in CMAQ was used to mark the five emission sections (agriculture, industry, energy, residents, and transportation) in the MEIC list [66] in order to analyze the contributions of $PM_{2.5}$ from different industries in the eastern region to each region, and to analyze the source characteristics of $PM_{2.5}$ by industry in the eastern region during and around New Year's Day.

This study adopted single-layer simulations, and the simulation area was shown in Figure 1b. It covered the eastern part of China, and the grid resolution was 36 km. The horizontal simulation area of WRF was slightly larger than that of CMAQ to ensure the accuracy of the boundary meteorological field, with simulation grids of 136×100 and 119×83, respectively. The Lambert conformal conic projection was used in the model. The two true latitudes were $30°$ N and $60°$ N, respectively.

2.3. Statistical Analyses

For the analysis of inference and trends, the independent samples t test was used for intergroup comparison to determine whether there was a significant difference in the mean values between the two groups [67]. This study's object was pollutant data from two different periods (such as the percentage increase in $PM_{2.5}$ on 2 and 3 January, and the contribution of industrial sources to $PM_{2.5}$ before and during the New Year's Day holiday). The level of significance was set at 0.05. The program called SPSS (Statistical Product and Service Solutions) for Windows (23.0, SPSS Inc., Chicago, IL, USA) was used. In addition, this study used standard deviation to describe the degree of dispersion of the data.

2.4. The Technical Workflow

The technical roadmap of this study is shown in Figure 2. Based on observational data and statistical analyses, the spatiotemporal distribution patterns of $PM_{2.5}$ during and around the New Year's Day holiday from 2015 to 2022, as well as the impacts of meteorological conditions on the pollution process, were studied. It was found that $PM_{2.5}$ had significant New Year's Day effects from 2019 to 2022. Then, we selected the year 2022 and used the WRF-CMAQ model to study the impacts of human activities on $PM_{2.5}$, evaluating the simulation performances. An industry source analysis was conducted using ISAM. The results in Sections 3.3 and 3.5 explained the reason why $PM_{2.5}$ had the New Year's Day effects it did.
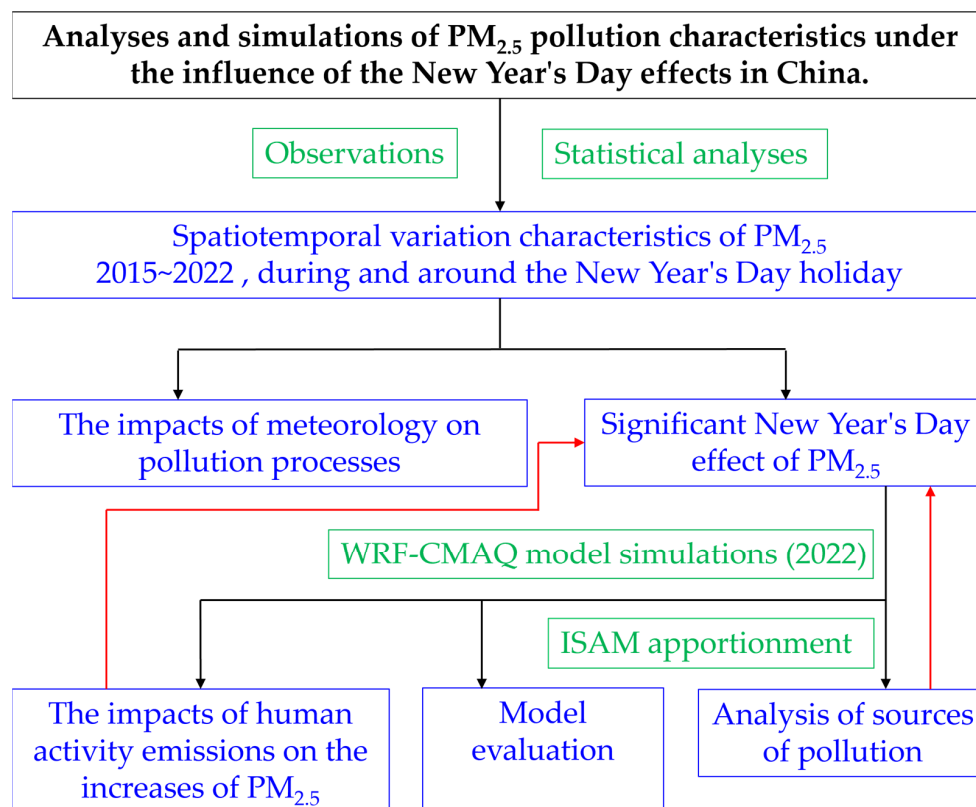
Figure 2. The technical roadmap. The results are represented by blue boxes and fonts, with green representing the methods, tools, or data used.

3. Results

3.1. Observation-Based Spatiotemporal Variation Characteristics of PM$_{2.5}$

3.1.1. Temporal Variation Characteristics

Figure 3 shows the average concentration changes in PM$_{2.5}$ levels in China for the entire study time from 2015 to 2022. As can be seen, the average PM$_{2.5}$ concentrations for the entire study time from 2015 to 2022 were 97.2 ± 34.3, 98.3 ± 43.0, 105.9 ± 58.2, 81.5 ± 29.9, 51.2 ± 19.3, 54.2 ± 19.9, 46.7 ± 15.7, and 56.5 ± 22.2 μg/m^3, respectively, showing an overall downward trend with a decline rate of 41.9%. This indicates that, under the strict implementation of air pollution prevention and control measures, the quality of the atmospheric environment in China has been significantly improved. Specifically, the average mass concentrations of PM$_{2.5}$ during (before and after) the New Year's Day holiday from 2015 to 2022 were 83.4 (84.9 and 129.8), 97.3 (109.1 and 83.2), 78.9 (114.7 and 120.6), 95.0 (88.2 and 58.7), 30.6 (48.9 and 74.9), 20.7 (33.7 and 67.5), 26.2 (42.5 and 65.4), and 45.4 (58.6 and 64.3) μg/m^3, respectively. From 2015 to 2018, the average PM$_{2.5}$ concentration for the entire study time in China exceeded the national secondary standard (75 μg/m^3). However, from 2019 to 2022, it remained below the standard and showed an upward trend from before until after the New Year holiday, with peaks occurring after the holiday.

Figure S1 shows the exceeding rates of PM$_{2.5}$ concentrations in 31 administrative cities in China for the entire study time. It can be seen that in heavily polluted years from 2016 to 2018, the exceeding rates during the New Year holiday were the highest in three time periods, while from 2019 to 2022, the rates were the highest after the New Year holiday. In some cities (such as Nanchang, Jinan, Zhengzhou, Wuhan, etc.), the exceeding rates before the New Year holiday were less than 0.2, while after the New Year holiday, the exceeding rates were greater than 0.6.
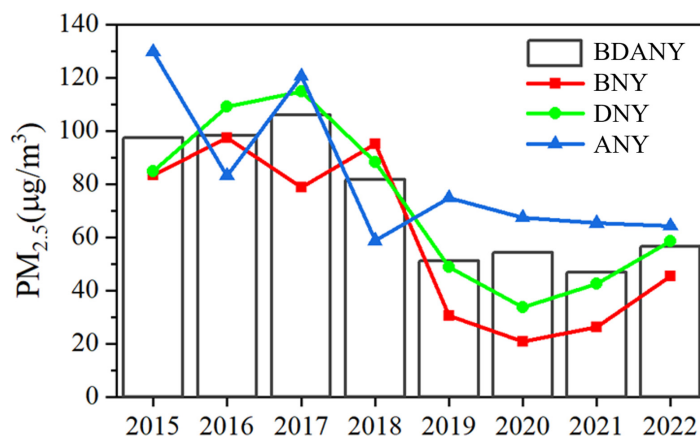
Figure 3. Changes in the average PM$_{2.5}$ concentrations nationwide for the entire study time (i.e., before, during, and after the New Year's Day holiday) from 2015 to 2022. BDANY: before, during, and after the New Year's Day holiday. BNY: before the New Year's Day holiday. DNY: during the New Year's Day holiday. ANY: after the New Year's Day holiday.

PM$_{2.5}$ concentrations in China were relatively high during and around the New Year holiday from 2015 to 2018. However, from 2019 to 2022, PM$_{2.5}$ concentrations decreased, and the New Year's Day effect was significant. That is to say, PM$_{2.5}$ concentrations gradually increased from before the New Year's Day holiday until after the New Year's Day holiday, reaching their peaks after the holiday.

3.1.2. Spatial Variation Characteristics

The concentrations of PM$_{2.5}$ are significantly affected by regional differences, which are mainly influenced by comprehensive factors such as different meteorological conditions, air pollution prevention and control measures, and energy and industrial structures [30,68]. Figure 4 shows the concentration differences during and around New Year's Day holiday in 2016 and 2022. It can be seen that the periods with the largest difference were during the New Year's Day holiday, followed by before the holiday. This may be due to frequent human activities during the New Year's Day holiday in 2016, resulting in higher concentrations of PM$_{2.5}$. Affected by the prevention and control of the COVID-19, the increases in PM$_{2.5}$ concentrations during the New Year's Day holiday in 2022 were lower than those in previous years. The regions with significant differences were mainly concentrated in BTHS, YRD, and central China. The specific spatial distributions of PM$_{2.5}$ concentrations each year are discussed below.

Figures S2 and S3 show our statistical analysis of the nationwide spatial distributions of PM$_{2.5}$ concentrations during the New Year's Day holiday from 2015 to 2022. It shows that PM$_{2.5}$ concentrations in mid-latitude cities were generally higher than those in high- and low-latitude cities, while PM$_{2.5}$ concentrations in Xizang, Inner Mongolia, South China, and some border areas were relatively low. The areas with higher PM$_{2.5}$ concentrations were mainly located in BTHS, YRD, and the central China region. BTHS and YRD had the most significant improvements in PM$_{2.5}$ concentrations, while the central China region still experienced mild pollution. Since 2019, the average concentrations of PM$_{2.5}$ have significantly decreased in most regions during and around the New Year's Day holiday, and the coverage of areas that meet the National Ambient Air Quality Secondary Standard has been expanding year by year.

From the observational data, it can be seen that the areas with high average PM$_{2.5}$ values from 2015 to 2018 were mainly located in the Beijing–Tianjin–Hebei, the Shandong Peninsula, and the Yangtze River Delta urban agglomerations. The Guanzhong urban agglomeration in Shaanxi and the Henan region has been affected by PM$_{2.5}$ transported from these heavily polluted areas. Meanwhile, due to their low altitude and distance from the sea, PM$_{2.5}$ concentrations in these regions have consistently been at a high level.

Except for the Anhui, Gansu, Guangdong, Jiangxi, Liaoning, Shaanxi, and Shanxi provinces, $PM_{2.5}$ concentrations during and around New Year's Day holiday in the other regions showed a downward trend. For example, $PM_{2.5}$ concentrations declined by $45.6 \pm 4.3\%$, $47.8 \pm 5.8\%$, $58.3 \pm 6.9\%$ in Guizhou, Shanghai, and Chongqing, and by $32.5 \pm 2.4\%$ to $36.1 \pm 2.3\%$ in Heilongjiang, Inner Mongolia, Sichuan, and Yunnan. On the other hand, they increased by $55.6 \pm 5.2\%$, $12.6 \pm 3.7\%$, $11.0 \pm 8.5\%$, $15.9 \pm 4.6\%$, $34.3 \pm 7.5\%$, $54.7 \pm 4.5\%$, and $26.1 \pm 9.7\%$ in Anhui, Gansu, Guangdong, Jiangxi, Liaoning, Shaanxi, and Shanxi, respectively. From 2016 to 2018, the number of $PM_{2.5}$ compliant cities increased from 145 to 163 out of 369 cities.
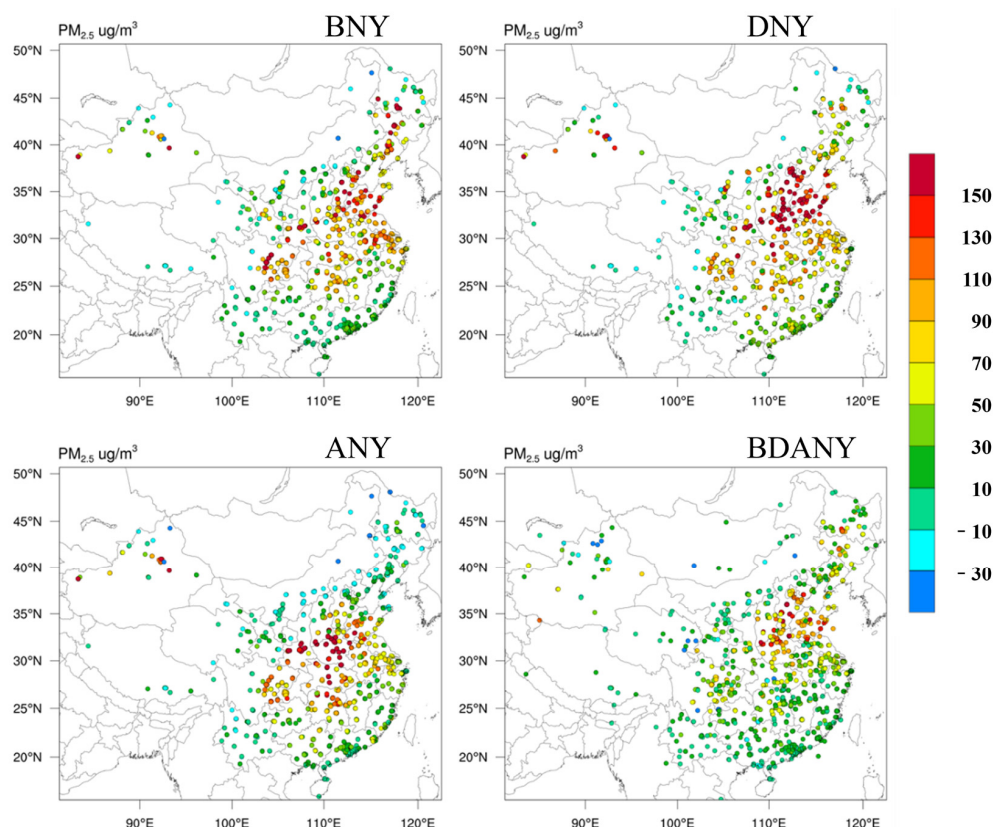

Figure 4. The difference in the average $PM_{2.5}$ concentration nationwide for the entire study time (i.e., before, during, and after the New Year's Day holiday) in 2016 and 2022. BDANY: before, during, and after the New Year's Day holiday. BNY: before the New Year's Day holiday. DNY: during the New Year's Day holiday. ANY: after the New Year's Day holiday. The dots represent the observed values of the corresponding areas.

From 2019 to 2022, the observed $PM_{2.5}$ concentrations during and around the New Year's Day holiday showed the following pattern: after the New Year's Day holiday > during the New Year's Day holiday > before the New Year's Day holiday. The results indicate that in the first stage (before the New Year's Day holiday), pollution in Xinjiang was relatively severe. Xinjiang is located in the northwest of China, and Urumqi and its surrounding cities are located in river valleys and basins. The special closed terrain can lead to calm winds and temperature inversion, conditions which are not conducive to the diffusion of pollutants. During the second stage (during the New Year holiday), the polluted areas gradually expanded, and pollution began to appear in Shaanxi, Henan, Shanxi, and Shandong regions. On the one hand, this was due to the expansion of pedestrian flow between cities, frequent travel activities, and a significant increase in motor vehicle commuting during the New Year holiday, factors which resulted in an increase in $PM_{2.5}$ emissions generated by human activities. On the other hand, the Fenwei Plain is located between mountains and plateaus, and the terrain and meteorological factors can also lead to the accumulation

of pollutants. In the third stage (after the New Year holiday), pollution in the Shaanxi, Henan, Shanxi, and Shandong regions continued to worsen. Compared to the second stage, $PM_{2.5}$ concentrations in this stage increased by 53.1%, 100.2%, 5.6%, and 9.8% in Shaanxi, Henan, Shanxi, and Shandong, respectively, with the addition of polluted areas in Hunan and Hubei also observed.

The concentrations of $PM_{2.5}$ under the New Year's Day effect varied in different regions, with higher concentrations in mid-latitude regions. $PM_{2.5}$ concentrations in Anhui, Gansu, Guangdong, Jiangxi, Liaoning, Shaanxi, and Shanxi increased after the New Year holiday from 2015 to 2018, while they decreased in other cities. The BTHS, YRD, and central China regions had the largest increases in $PM_{2.5}$ from 2015 to 2018 and were the areas most affected by the New Year's Day effects. In addition, $PM_{2.5}$ easily accumulated in the Shaanxi, Henan, Shanxi, and Shandong regions.

3.2. Model Evaluation

3.2.1. Assessment for Simulated Pollutant Concentrations

As shown in Figure 5, Case17 performed its simulation well during the cleaning period, and the simulated values showed spatiotemporal distribution trends that were close to the observed values. The simulation results of Case16 showed a certain degree of overestimation in the BTHS, YRD, and Southwest (SW) regions, with simulation values approximately 40~90% higher than the observed values. During the periods of pollution onset and worsening, Case16 accurately captured high $PM_{2.5}$ concentrations in YRD, FWP, and central China, especially on 3 and 4 January. However, Case17 did not capture this pollution event and underestimated it by over 100 $\mu g/m^3$.

Before the New Year holiday in 2022, there was almost no regional pollution in the eastern regions. After the holiday, regional pollutions emerged, and over time, the pollution continued to worsen. On 1 January, BTHS first experienced mild-to-moderate pollution, with $PM_{2.5}$ concentrations ranging from around 100~130 $\mu g/m^3$. On 2 January, $PM_{2.5}$ in BTHS significantly decreased, while $PM_{2.5}$ in Anhui, Henan, and Hubei regions increased, reaching a maximum of 150~170 $\mu g/m^3$, and mild pollution began to appear in the YRD area, ranging from around 100~120 $\mu g/m^3$. On 3 January, the pollution range expanded, and the pollution concentrations also increased. The $PM_{2.5}$ concentrations in some areas of Henan and Hubei reached over 180 $\mu g/m^3$, and rose to 110~140 $\mu g/m^3$ in YRD. On 4 January, the pollution ranges further spread southward and westward, and the pollution in the Shaanxi and Hunan regions worsened, with levels in some areas rising to over 180 $\mu g/m^3$. On 5 January, the concentrations of $PM_{2.5}$ significantly decreased, and severe pollution was mainly concentrated in the Guanzhong area of Shaanxi. The pollution in YRD receded, while mild-to-moderate pollution still existed in the Henan and Hubei regions.

Figure 6 shows the time series comparison of observed $PM_{2.5}$ values (OBS) and simulated values (Case16 and Case17), with results obtained using the different emission inventories for 22 cities (Beijing, Fuzhou, Hangzhou, Hefei, Jinan, Nanchang, Nanjing, Shanghai, Shijiazhuang, Taiyuan, Tianjin, Wuhan, Zhengzhou, Luoyang, Nanyang, Xinyang, Jiaozuo, Luohe, Xiangyang, Jingzhou, Liaocheng, and Heze) for the entire study time. It can be seen from Table S1 that the $PM_{2.5}$ concentrations in Beijing, Tianjin, and Shijiazhuang are relatively low for the entire study time. Case16 shows varying degrees of overestimation, while Case17 shows better simulation results. In Case17, the normalized mean bias (NMB) (and normalized mean error (NME)) values for Beijing, Tianjin, and Shijiazhuang were 30.2% (20.7%), 9.9% (14.5%), and 7.4% (18.8%), respectively. Tianjin, Beijing, and Shijiazhuang met the performance benchmarks ($\leq\pm15\%$) [69,70]. The R values in the three cities were 0.82, 0.86, and 0.62, respectively, indicating that the model simulated the trends of $PM_{2.5}$ pollution change well. From the time series chart, it can be seen that Case17 underestimated the observed $PM_{2.5}$ values of the other 19 cities to varying degrees. Case16 produced good simulations of the trends in $PM_{2.5}$ concentration change during and before the New Year's Day holiday. The model could simulate most $PM_{2.5}$ pollution processes and had good reproducibility for most concentration peaks. In Case16, the model overestimated

PM$_{2.5}$ concentrations in Jinan, Zhengzhou, Liaocheng, and Heze before the New Year's Day holiday, while simulating the pollution peaks during and after the New Year's Day holiday better. The NMB values in Hangzhou, Hefei, Jinan, Nanchang, Nanjing, Zhengzhou, Luoyang, Nanyang, Xinyang, Jiaozuo, Luohe, Xiangyang, Jingzhou, Liaocheng, and Heze were all within the standard target range. Only Fuzhou, Shanghai, Wuhan, and Taiyuan exceed the benchmarks, with NMB values of −23.9%, −25.7%, 37.5%, and 23.6%, respectively. From the perspective of correlation coefficients, the model simulated PM$_{2.5}$ levels well in 19 cities, except for Fuzhou, Jinan, and Heze, with an R value greater than 0.6. Based on the above analysis, compared with the evaluation standards recommended by the US Environmental Protection Agency, the simulation errors of Case16 for nineteen heavily polluted cities were within an acceptable range (NME $\leq$ 50%), which basically reflected the sustained trends in heavy pollution processes and ensured the reliability of the results of the analysis of PM$_{2.5}$ pollution characteristics and formation processes.
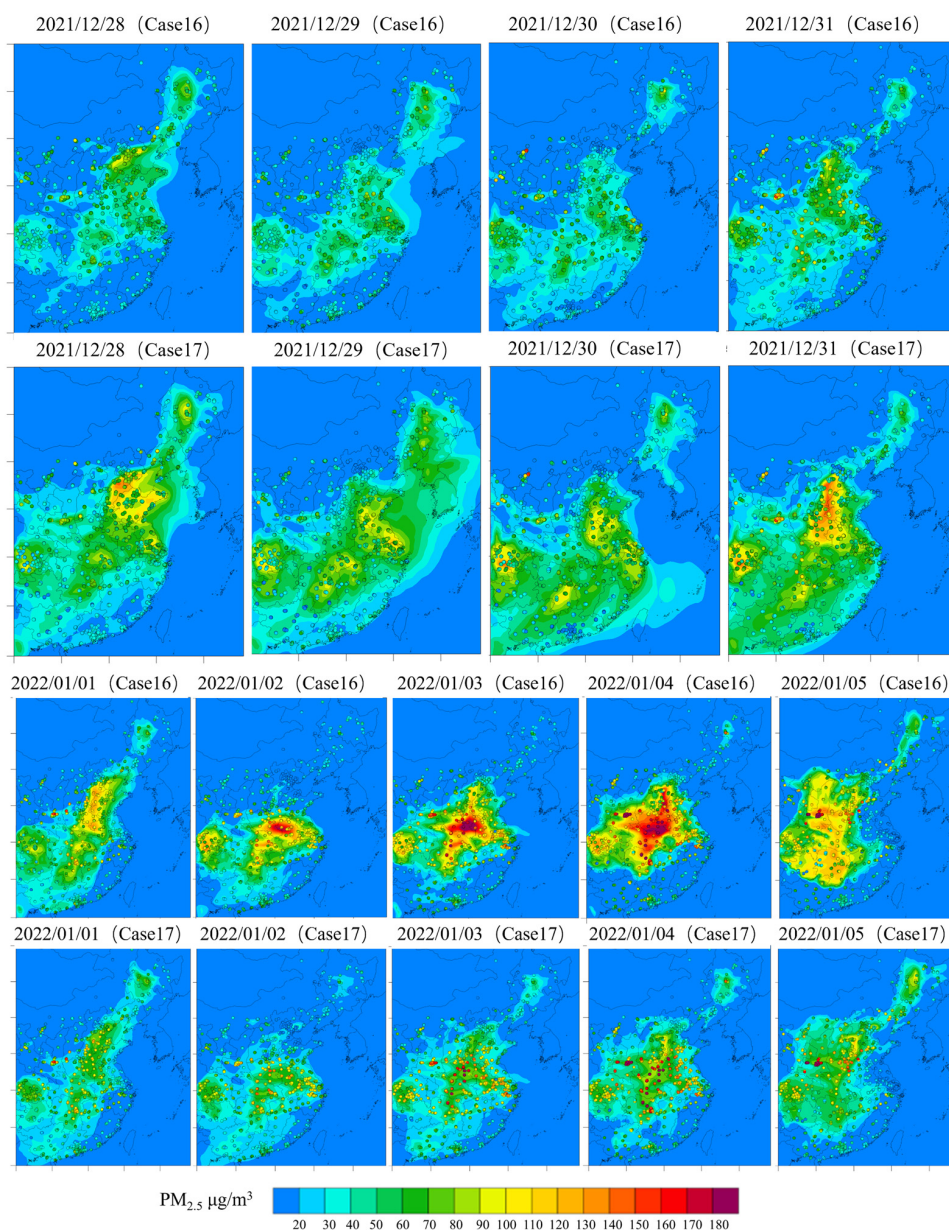

Figure 5. Temporal and spatial distributions of the simulated PM$_{2.5}$ concentrations in the eastern region, as determined using different emission inventories before the New Year holiday (clean period, first 8 images), for during and after the New Year holiday (pollution period, last 10 images). The dots represent the observed values of the corresponding areas.
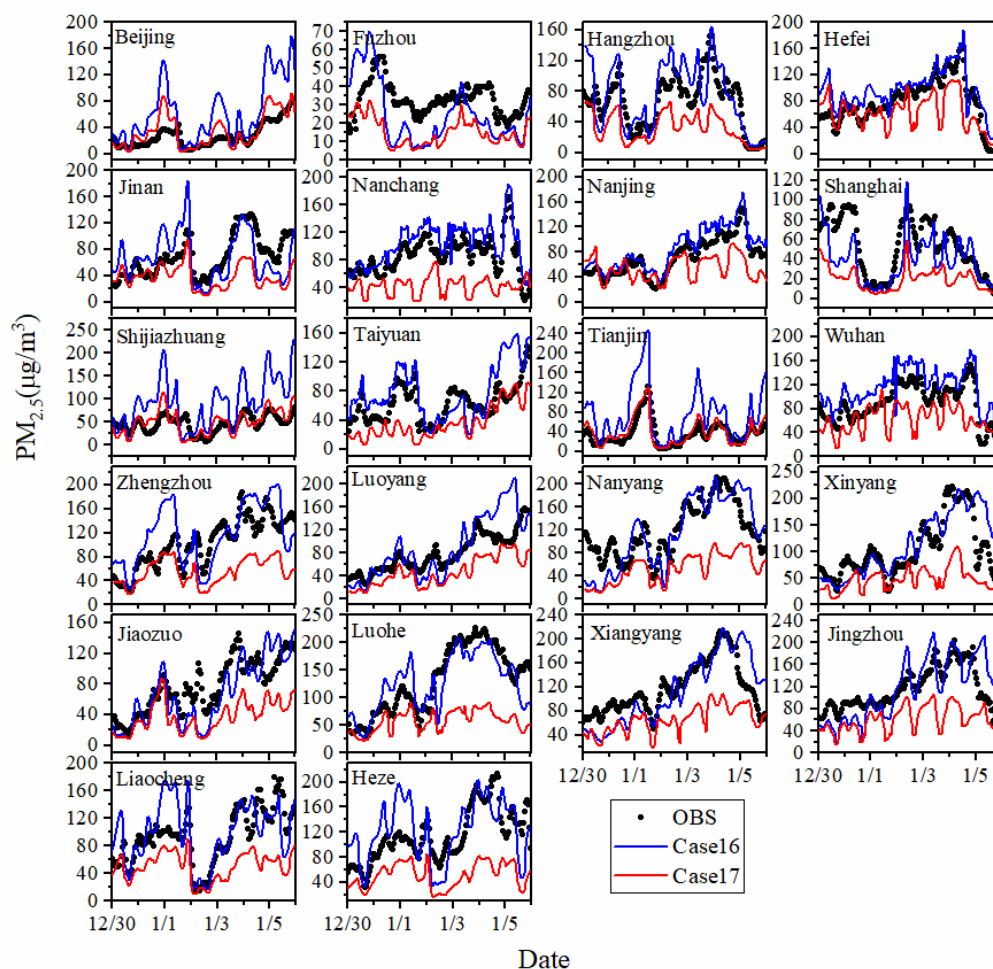
Figure 6. Comparison of simulated and observed values of PM$_{2.5}$ using different emission inventories in 22 cities. OBS: observed data. Case16: values simulated using the 2016 emission inventory. Case17: values simulated using the 2017 emission inventory.

3.2.2. Assessment of Simulated Meteorology

We conducted pattern evaluation analysis on five meteorological parameters (i.e., temperature (T), humidity (RH), wind speed (WS), wind direction (WD), and air pressure (P)) in twelve key cities (Jinan, Taiyuan, Zhengzhou, Luoyang, Nanyang, Xinyang, Jiaozuo, Luohe, Xiangyang, Jingzhou, Liaocheng, and Heze). Figures S4–S6 show the results of time series comparisons of simulated and observed meteorological parameters for these cities. Table S2 presents the statistical evaluation results of the five main meteorological parameters.

From the evaluation results, it can be seen that the model captured the changes in temperature well. The mean bias (MB) values in Taiyuan, Luoyang, Xinyang, Liaocheng, and Heze were all smaller than the reference standards (≤±0.5), with values of 0.04, −0.12, −0.12, 0.11, and 0.16 °C, respectively. The change trends of simulated temperature values in 12 cities were also in good agreement with the observed values, and the R values were higher than 0.85. The model captured the trends of humidity changes in the twelve cities well, with R values greater than 0.87 in all cities except Taiyuan, Xiangyang, and Jingzhou. As far as R values were concerned, the simulated ground wind speed values were in good agreement with the observed values. The model simulates the trends in wind direction change in some cities well, such as Jinan, Zhengzhou, Luoyang, and Xinyang, where the R values were all greater than 0.5. Except for Xinyang, the mean error (ME) and the root-mean-square error (RMSE) values of the other cities met the benchmarks (≤±0.2) [71]. According to existing studies, the current poor simulations of ground wind directions by

meteorological models are a common problem, especially when it is difficult to directly compare simulated values with observed values for wind directions [71]. The overall simulations of P in the twelve cities were good, with MB, ME, and RMSE values all within ± 0.2. Its R values were the highest among the five meteorological factors, ranging from 0.9 to 0.97. This indicated a high degree of agreement between the simulated and observed values of air pressure.

Overall, the WRF meteorological model had an acceptable range of errors in the meteorological simulation results obtained for the twelve cities, ensuring the reliability of meteorological analysis and providing a reliable meteorological driving field for the CMAQ simulations.

3.3. The Impacts of Human Activity Emissions on the Increases in PM$_{2.5}$

From the simulation evaluations shown in 3.2.1, it can be concluded that during the clean period (here, we define the two days before the New Year holiday as the clean period), the observed concentrations of PM$_{2.5}$ were equivalent to the simulated level of Case17. Therefore, the PM$_{2.5}$ concentration level during the clean period could be assumed to correspond to the emission level of Case17. Perhaps due to human activities during the New Year's Day holiday, especially increases in traffic emissions caused by the large number of motor vehicles in use, and other factors, the PM$_{2.5}$ concentrations increased significantly. The PM$_{2.5}$ concentration levels were equivalent to the simulated emission level of Case16. Therefore, from an emission perspective, the PM$_{2.5}$ concentrations during and after the holiday could be assumed to be equivalent to the emission level of Case16. Based on the above assumptions, due to the lack of other objective conditions for human activities to intervene, the emissions of pollutants before the holiday were at a normal level. Therefore, the concentrations of PM$_{2.5}$ were relatively low, and air pollution would not occur. Additionally, the PM$_{2.5}$ concentrations were low, which would not cause air pollution. After the holiday, human activities suddenly exploded, leading to increases in pollutant emissions and increases in atmospheric pollutant concentrations. So, without objective holiday interventions, PM$_{2.5}$ concentrations during and after the holiday should be maintained at the emission level of Case17, and the increases in PM$_{2.5}$ caused by human activities should be the differences between the emission levels of Case16 and Case17.

Figure 7 shows the spatiotemporal distributions of the increases in PM$_{2.5}$ concentrations caused by human activities, with values calculated based on the differences between the emission levels of Case16 and Case17. It can be seen that on 1 January, at the beginning of the holiday, the PM$_{2.5}$ concentrations in BTHS increased significantly, at around 65~85 $\mu g/m^3$, while in the rest of the eastern region, the increases were by about 35~65 $\mu g/m^3$. On 2 January, the increases occurred in the YRD and central China regions, especially in the Anhui, Hubei, and Henan regions, with average increases of 95.56, 62.36, and 65.25 $\mu g/m^3$, respectively. On 3 January, the scope of increases in central China expanded and the number of increases was enhanced. The average increases in the Henan, Hubei, and Hunan regions were 96.25, 70.28, and 47.14 $\mu g/m^3$, respectively. The increases in Hebei, Shandong, and Jiangsu also increased significantly, especially in the southern Hebei and western Shandong regions, with some areas experiencing a maximum increase of 75 to 95 $\mu g/m^3$. On 4 January, the increases in PM$_{2.5}$ concentrations spread from Henan to the surrounding areas, expanding the ranges affected and increasing the amounts they are affected by. For the north to the BTHS regions, the PM$_{2.5}$ concentration increased by 85~105 $\mu g/m^3$. For areas from the south to the Hunan–Hubei regions, the highest increases were around 75~85 $\mu g/m^3$. For the west to CDCQ, east to the northern Anhui and western Shandong regions, the increases were 75~95 $\mu g/m^3$. On 5 January, the scope of expansion extended southward, and the increases in YRD and BTHS regions decreased. Except for southern Anhui and northwestern Zhejiang, where the increases decreased to below 25 $\mu g/m^3$, there were basically no increases in other areas. The average increase in the Hebei region decreased to 46.18 $\mu g/m^3$. The areas with significant increases were mainly FWP and central China, and the enhancements decreased significantly compared to

the previous days. The average increases in Shaanxi, Shanxi, and Henan were 62.35, 38.89, and 44.52 μg/m^3, respectively, while the increases in Hubei, Hunan, and Jiangxi were 52.36, 61.25, and 37.26 μg/m^3, respectively.

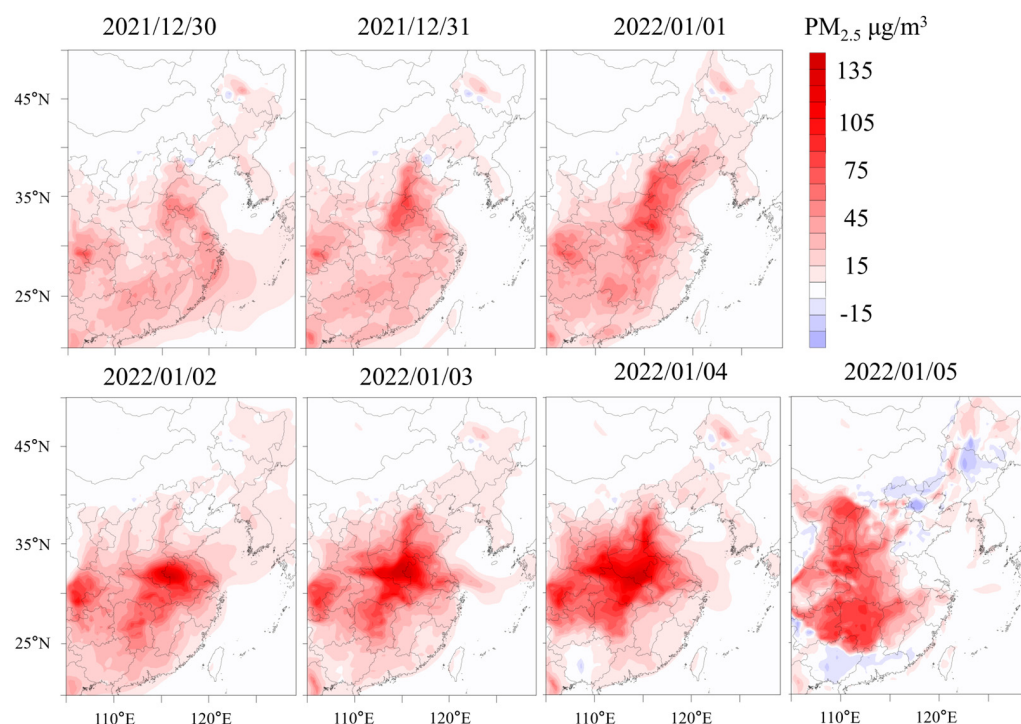**Figure 7.** Spatiotemporal distribution maps of simulated differences in PM$_{2.5}$ between Case16 (using the 2016 emission inventory) and Case17 (using the 2017 emission inventory) in the eastern region.

To quantitatively analyze the characteristics of PM$_{2.5}$ concentration increases caused by human activities, a time series analysis of PM$_{2.5}$ concentration increases was conducted in twelve key study cities, as shown in Figure 8. It can be seen that the peak increases in PM$_{2.5}$ concentrations in Zhengzhou, Luoyang, Xinyang, Jiaozuo, Luohe, Xiangyang, Jingzhou, Liaocheng, and Heze occurred from 4 to 5 January. Among these area, Xinyang had the largest increase, with the highest reaching 175.26 μg/m^3. The peak increases in Zhengzhou, Luoyang, Luohe, Xiangyang, Jingzhou, and Heze ranged from 110 to 130 μg/m^3, and the increases in Liaocheng ranged from 70 to 90 μg/m^3. Additionally, Jinan, Taiyuan, Zhengzhou, Liaocheng, and Heze also experienced peak PM$_{2.5}$ increments during the first holiday, with increments in Taiyuan and Heze ranging from 100 to 120 μg/m^3. The increments seen in Jinan, Zhengzhou, and Liaocheng range from 80 to 100 μg/m^3. The peak values of PM$_{2.5}$ concentration increments in Jinan, Taiyuan, Zhengzhou, Luoyang, Nanyang, Xinyang, Jiaozuo, Luohe, Liaocheng, and Heze all appeared on 2 January and were all below 10 μg/m^3. From the perspective of percentage increases, compared with 2 January, all cities saw significant increases on 3 January ($p = 0.03$) and maintained a relatively high level ($1.3 \pm 0.6\%$). Under the influences of increased human activities, the concentrations of PM$_{2.5}$ increased during and after the New Year's Day holiday.
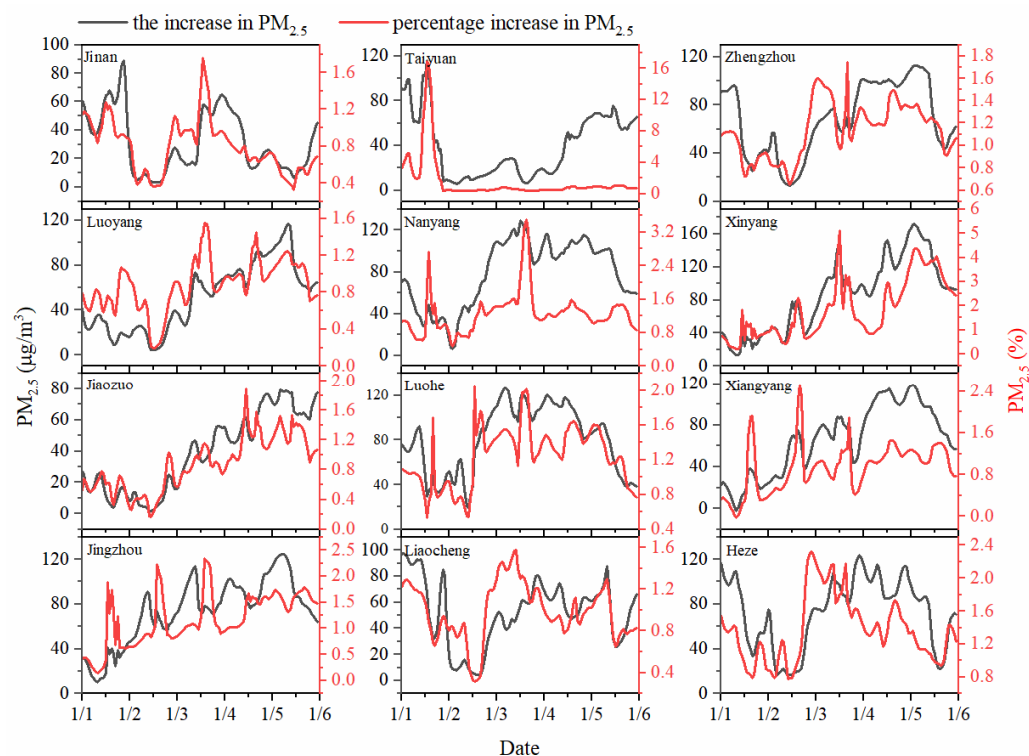
Figure 8. The increases (Case16–Case17) and percentage increases ((Case16–Case17)/Case17) in $PM_{2.5}$ concentrations in 12 heavily polluted cities (Jinan, Taiyuan, Zhengzhou, Luoyang, Nanyang, Xinyang, Jiaozuo, Luohe, Xiangyang, Jingzhou, Liaocheng, and Heze).

3.4. The Impacts of Meteorology on Pollution Processes

Figure 9 and Figure S7 show the evolution of near-surface temperature, wind speed, and ground pressure (obtained from FNL data) in eastern China and its surrounding areas during and around New Year's Day in 2022. In the early stage of the pollution process (08:00 on the 30 and 31 December 2021), the central and eastern regions were affected by the Siberian high pressure in Mongolia, which brought cold currents and lower temperatures. A high-pressure center was formed in central China, and the eastern region was mainly controlled by weak high pressure due to the influence of anticyclonic airflow. The isobars were dense, and the winds were relatively strong. Overall, no favorable conditions were provided for the accumulation of pollutants. As of 08:00 on the 1 January 2022, the southeast region was dominated by westerly airflow, while the northeast region was dominated by northwest airflow, which was conducive to transporting $PM_{2.5}$ from the Hebei, Shaanxi, and Henan regions to the western Shandong region. The eastern region was generally in a weak high-pressure range, and the weak wind speed within the high-pressure range provided favorable conditions for the accumulation of pollutants. Therefore, the accumulation of $PM_{2.5}$ in the western region of Shandong Province was prominent. During the holiday period (08:00 on the 2 January 2022), the high-pressure center moved northward and formed a low-pressure center in the western region. The Henan and Anhui regions were on the edge of weak high-pressure in the north, with sparse isobars and low wind speeds, which were not conducive to the diffusion of pollutants. Therefore, moderate pollution occurred in the central region of China, especially in the Henan, Hubei, and Anhui regions, with $PM_{2.5}$ concentrations reaching around 120 μg/m³. By 08:00 on the 3 January 2022, the Siberian high-pressure system in Mongolia brought a strong cold air mass, with cold air approaching from north to south. The dry and cold northwest winds transported $PM_{2.5}$ southward in the BTHS region. In the central and eastern regions, the isobars were sparse, the airflow was stable, and the wind speed remained relatively calm, providing very favorable conditions for the accumulation of the pollutants transported. Therefore, the

pollution ranges in central China expanded, with Henan as the center, north to Hebei, south to Hunan, and east to Zhejiang. The highest concentrations of PM$_{2.5}$ reached 220 μg/m^3. By 08:00 on the 4 January 2022, the cold air was moving southward, and due to the influence of the cold front, precipitation began to occur in the central and eastern regions. Moreover, the low air pressure and dense isobars increased the northerly wind speeds. With the support of cyclonic airflow, the polluted areas also began to move southward, causing a decrease in pollution concentrations in the Hebei region, while pollution in central China, especially in the Hubei and Hunan regions, intensified. By 08:00 on the 5 January 2022, the isobars in the eastern region were dense, with strong winds and relatively high air pressures. Influenced by anticyclonic airflow, pollution began to gradually decrease with the continuous support of northerly airflow, and the levels in the central and eastern regions began to drop to below 120 μg/m^3.
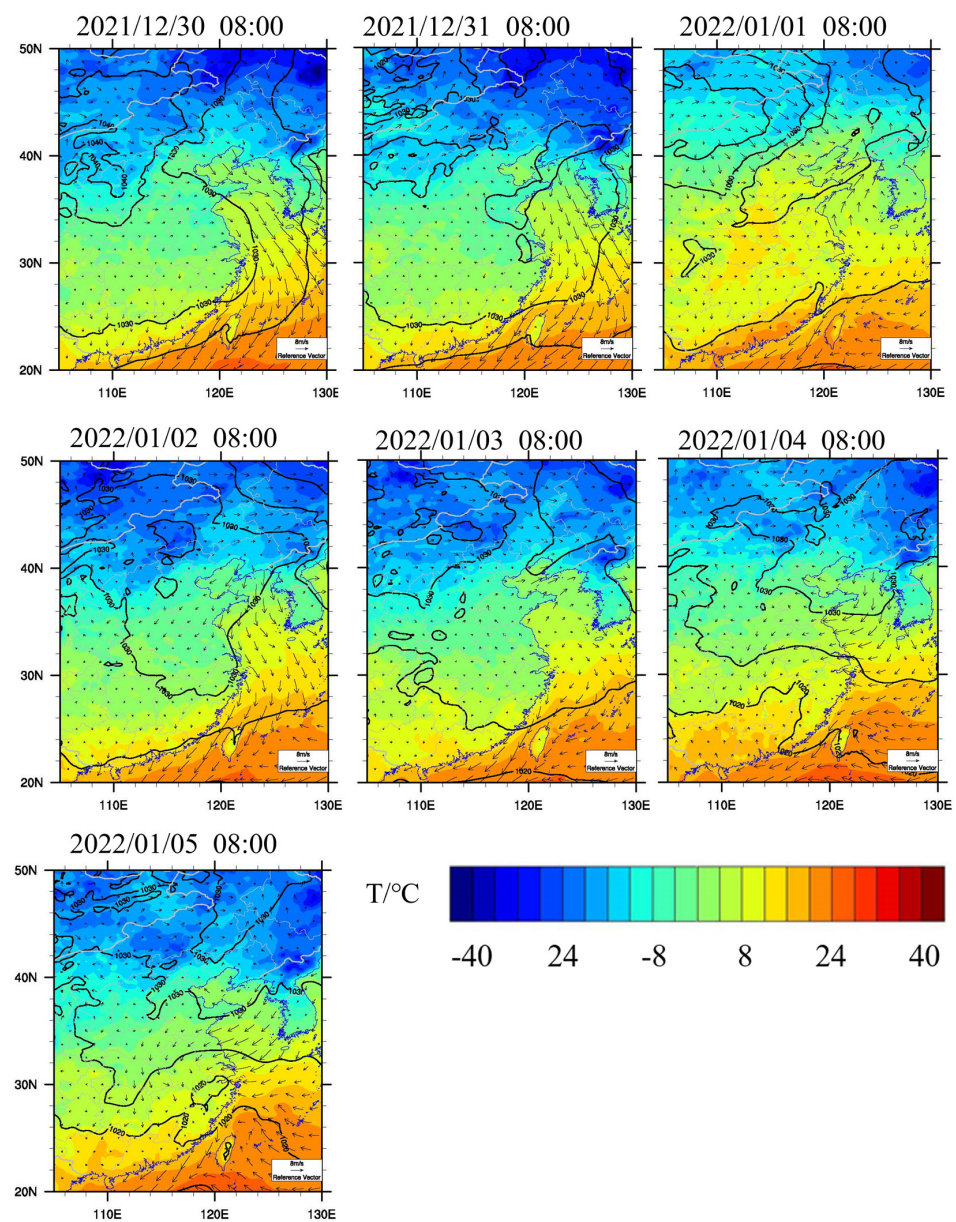

Figure 9. The evolution of near-surface temperature (shadow, °C), wind fields (arrow, m/s), and sea level pressures (contour line, hPa) at 08:00 from 30 December 2021 to 5 January 2022.

Based on meteorological data taken from seven days (during and around the New Year's Day holiday) in 2022, the characteristics of various meteorological elements in

different time periods and the frequencies of various weather occurrences in different time periods were statistically analyzed. The results are shown in Table 1 and Table S3. The temperatures in eleven cities of the cities, but not in Jingzhou, were the lowest after New Year's Day, indicating that high PM$_{2.5}$ concentrations occurred at lower temperatures. In this study, the relative humidity of the twelve cities showed the following pattern over three periods: BNY (44.8 ± 11.7%) < DNY (52.1 ± 8.5%) < ANY (78.6 ± 13.3%). This result is consistent with the variation patterns of PM$_{2.5}$ concentrations. The humidity increased with the aggravation of pollution. After New Year's Day, the average humidity reached 78.62% when the pollution was the heaviest. The humidity in Zhengzhou, Nanyang, Xiangyang, Luoyang, Xinyang, Luohe, Liaocheng, and Heze exceeded 80%. In Jinan, Zhengzhou, Jiaozuo, Liaocheng, Taiyuan, Luoyang, and Heze, wind speeds decreased with increasing pollution. The average wind speeds after New Year's Day were 0.33 m/s, indicating that the weakened wind speeds reduced the diffusion capacity of pollutants. However, Nanyang, Xiangyang, Xinyang, Luohe, and Jingzhou had higher wind speeds during the heavily polluted stages, indicating that the PM$_{2.5}$ concentrations in these cities were heavily affected by regional transport activity during the heavily polluted stages. The air pressure was generally low during the heavy-pollution stages. From the perspective of accompanying weather phenomena, during the period of no pollution or light pollution before the New Year holiday, the proportion of sunny days was basically around 50%, and the proportion of accompanying cloudy days was around 25%. But when pollution occurred, the proportion of sunny days decreased, while the proportions of cloudy and rainy days increased significantly. This indicates that weak precipitation had limited effects on improving air quality, but was actually beneficial for the growth of PM, exacerbating pollution. Meteorological conditions such as temperature, wind speed, air pressure, and relative humidity affect the formation of PM$_{2.5}$.

Table 1. The frequencies of various weather occurrences in different time periods (before/during/after New Year's Day, %).

City	Clear Day	Cloudy Day	Overcast Sky	Rainy Day
Jinan	75/85/48	25/15/8	0/0/44	0/0/0
Taiyuan	48/82/18	31/25/44	21/0/38	0/0/0
Zhengzhou	36/82/0	37/18/10	27/0/23	0/0/67
Luoyang	50/94/0	25/6/23	25/0/52	0/0/25
Nanyang	63/74/0	12/16/29	25/10/52	0/0/19
Xinyang	75/83/0	25/17/0	0/0/40	0/0/60
Jiaozuo	48/88/0	2/12/4	50/0/69	0/0/27
Luohe	35/72/2	40/28/20	25/0/41	0/0/37
Xiangyang	63/100/23	37/0/0	0/0/62	0/0/15
Jingzhou	50/65/0	50/35/0	0/0/81	0/0/19
Liaocheng	73/87/12	27/13/35	0/0/46	0/0/7
Heze	54/87/0	46/13/6	0/0/56	0/0/38

3.5. Analysis of Sources of Pollution

Figure 10 shows the distributions of the PM$_{2.5}$ concentrations contributed by various industries during and around New Year's Day in 2022. The industries in the eastern region that contributed the most to PM$_{2.5}$ were residential and industrial sources, followed by transportation and energy sources, while agricultural sources contributed the least. The changes in the contributions of agricultural and residential sources were relatively small. Two days before the New Year holiday, 30 and 31 December 2021, the contributions of agricultural sources were relatively high in the central and northern regions, mainly in the northwest (Shaanxi, Ningxia, and Gansu), with the PM$_{2.5}$ concentrations generated ranging from 2.5 to 3 μg/m^3. On 1 and 2 January 2022, the contributions of agricultural sources began to spread eastward, and the contributions in the northwest region weakened relatively, averaging down to 2~2.5 μg/m^3. The contributions in Shanxi, Henan, and Hubei regions increased, with average contributions of 2~2.5 μg/m^3 in Shanxi and a maximum of

2.5~3 μg/m^3 in the Henan and Hubei regions. On the last day of the holiday and after the holiday (3~5 January 2022), the contributions in the BTHS, Jiangsu, and Shandong regions increased to 1.5~2.5 μg/m^3.
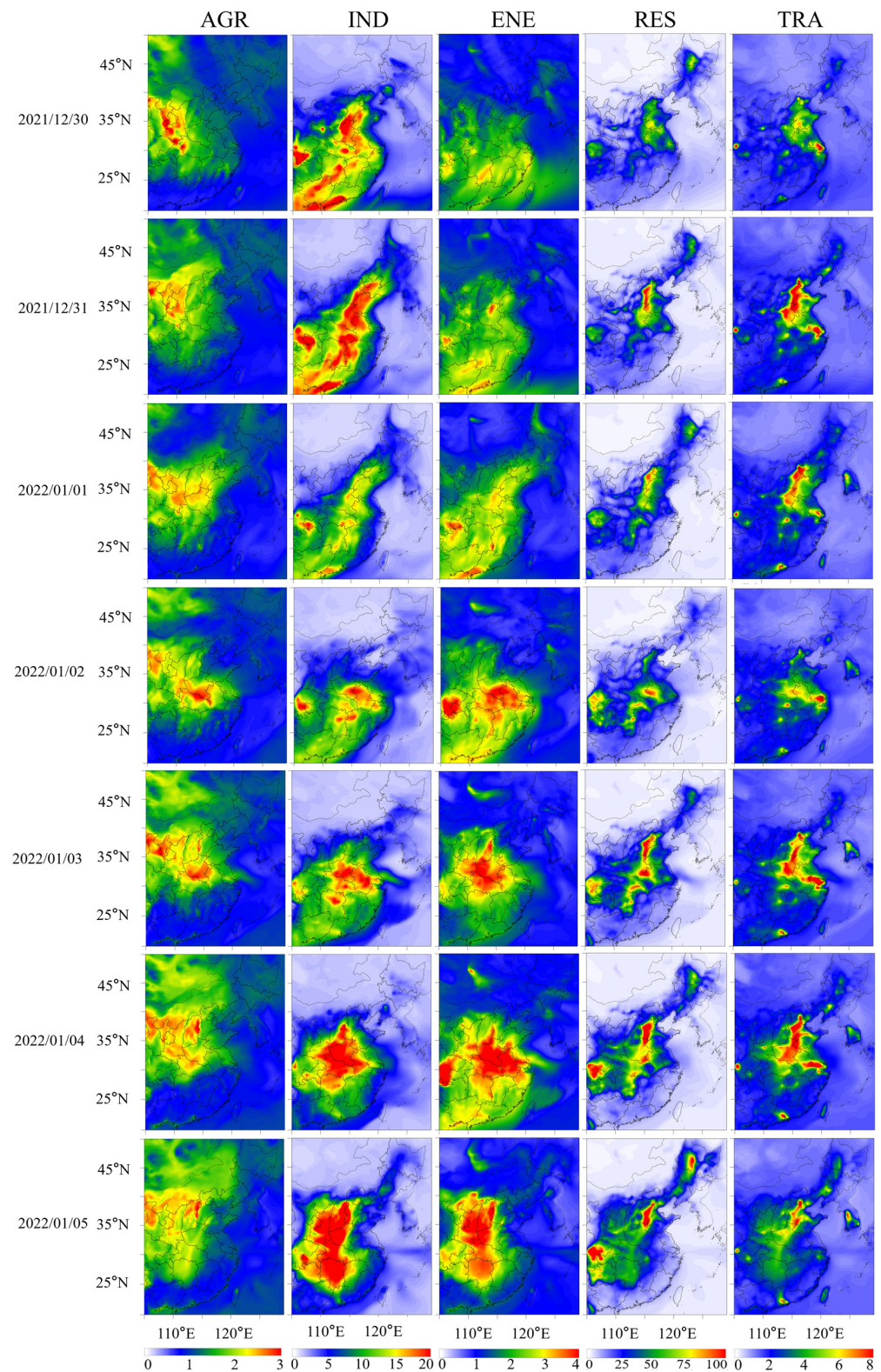

Figure 10. The daily average contributions of PM$_{2.5}$ by different sources in the eastern region from 30 December 2021 to 5 January 2022. AGR: agricultural source. IND: industrial source. ENE: energy source. RES: residential source. TRA: transportation source.

Before the New Year's Day holiday, $PM_{2.5}$ concentrations contributed by residential sources were relatively high in BTHS, Henan, Shandong, and Anhui, with an average of 70~75 $\mu g/m^3$. During the New Year holiday, the contributions in these areas, except Shandong, increased significantly, reaching a maximum of 90 to 100 $\mu g/m^3$ on 3 January. After the New Year holiday, the contributions in spatial distributions were similar to the levels seen before, but the concentrations decreased. On 5 January, except for BTHS, $PM_{2.5}$ concentrations in all other regions decreased to 60~70 $\mu g/m^3$, but there were increases in the Northeast region, and in the Heilongjiang region the contribution rose to 90~100 $\mu g/m^3$.

The $PM_{2.5}$ concentrations contributed by power sources varied significantly during and around New Year's Day, showing a gradual increase. Prior to the holiday, the overall concentrations in the eastern region were higher, especially in the Henan, Hunan, and Guangdong provinces, with the levels reaching highs of 3~4 $\mu g/m^3$ on the 31 December 2021. During the New Year holiday, $PM_{2.5}$ concentrations in FWP, YRD, and central China increased, reaching 3~4 $\mu g/m^3$ on 2 January. On 3 January, FWP reached 3~4 $\mu g/m^3$. After the New Year holiday, the contribution values in YRD decreased relatively, while the contribution areas in FWP and central China region significantly expanded.

The contributions of the $PM_{2.5}$ concentrations generated by industrial and transportation sources showed a significant pattern that constantly changed, reflecting human activity factors before and after the holiday. The concentrations of $PM_{2.5}$ from industrial sources were higher before and after the New Year holiday, while their values during the holiday period were significantly reduced (3.2 ± 1.6 $\mu g/m^3$, $p = 0.04$) due to some industrial shutdowns. Before the New Year holiday, the $PM_{2.5}$ concentrations contributed by industrial sources in the entire eastern region were relatively high. Except for the Jiangsu, Zhejiang, and Fujian regions, the concentrations in other regions reached 15~20 $\mu g/m^3$. The $PM_{2.5}$ concentrations contributed by industrial sources on 1 January were lowest during the entire study period, and the $PM_{2.5}$ contribution values in the eastern region basically decreased to 12~17 $\mu g/m^3$. On 2 January, the contribution range of industrial sources narrowed, being mainly located in YRD and central China, while emissions in the BTHS, Shandong, and Shanxi regions dropped to below 7 $\mu g/m^3$. After the New Year holiday, the concentration ranges of $PM_{2.5}$ generated by industrial sources began to spread westward and southward, with a significant decrease in YRD and Shandong regions, but significant increases in FWP, central and southern China, reaching over 20 $\mu g/m^3$.

The $PM_{2.5}$ concentrations generated by transportation sources were mainly higher in BTHS, Shandong, Henan, and YRD, with an average level of 5~6.5 $\mu g/m^3$ on the 30 December 2021. This reached a level of 7~8 $\mu g/m^3$ around Shanghai. On 31 December, 2021 and 1 January 2022, due to the holiday and frequent transportation, the concentrations of $PM_{2.5}$ increased, reaching 6~8 $\mu g/m^3$. After a brief decline on the 2 January, the $PM_{2.5}$ concentrations increased again on the 3 and 4 January due to the end of the holiday and frequent traffic. After the peak traffic period on the 5 January passed, the concentrations of $PM_{2.5}$ produced decreased again. The changes in industrial and transportation sources had led to differences in $PM_{2.5}$ before and after the New Year holiday.

4. Discussion

This paper analyzed the spatiotemporal variation characteristics of $PM_{2.5}$ during and around the New Year's Day holiday from 2015 to 2022 based on observational data. This study's scope was divided into nine regions in order to explore the changes in $PM_{2.5}$ caused by the New Year's Day effect in different regions. Based on numerical simulations, we focused on analyzing the causes of $PM_{2.5}$ pollution during and around the New Year's Day holiday in 2022. During and around the New Year's Day holiday from 2015 to 2022, the concentrations of $PM_{2.5}$ showed a downward trend, with a decline rate of 41.9%. This was consistent with the study of Feng et al. [72]. This indicated that under the strict implementation of air pollution prevention and control measures in China, the quality of the atmospheric environment had been significantly improved. After 2019, the $PM_{2.5}$ concentrations during and around the New Year's Day holiday in China all met the

national second-level standards (75 µg/m^3), but there was still a certain gap with the PM$_{2.5}$ safe daily average concentration standard value (25 µg/m^3) proposed by the World Health Organization (WHO), indicating the need for the further control of PM$_{2.5}$ pollution in China [73].

PM$_{2.5}$ concentrations were generally higher in mid-latitude cities, especially in BTHS, YRD, and central China, which might be related to pollution from heavy industry or insufficient environmental protection [74]. Due to the impact of the COVID-19 prevention and control, the PM$_{2.5}$ increase rates in BTHS, YRD, central China with busy industrial productions and economic prosperities decreased during the New Year's Day holiday in 2022. From 2015 to 2018, the Guanzhong urban agglomeration in Shaanxi and the Henan region had higher PM$_{2.5}$ concentrations, which might be due to their locations in plains and being more susceptible to transport effects from heavily polluted areas. Except for Anhui, Gansu, Guangdong, Jiangxi, Liaoning, Shaanxi, and Shanxi, where PM$_{2.5}$ concentrations increased (11.0~55.6%), all other provinces showed varying degrees of decline. From 2019 to 2022, this study observed the New Year's Day effects of PM$_{2.5}$ pollution in all cities, where PM$_{2.5}$ concentrations showed an increasing trend from before to after the New Year's Day holiday, with peaks occurring after the holiday. However, there were significant regional variations in PM$_{2.5}$ concentrations during different periods. Before the New Year's Day holiday, the relatively closed terrain conditions in Xinjiang made it difficult for PM$_{2.5}$ to spread, and the area was the first to see high PM$_{2.5}$ values. Subsequently, due to increased human activities and barriers from mountains and plateaus, PM$_{2.5}$ accumulated in Shaanxi, Henan, Shanxi, and Shandong regions during the holiday. Finally, after the holiday, human activities increased again, and PM$_{2.5}$ pollution continued to worsen in the aforementioned areas, spreading to the Hunan and Hubei regions. In summary, the spatial distribution characteristics of PM$_{2.5}$ indicated that the impacts of the New Year's Day effect on PM$_{2.5}$ concentrations in different regions seemed to be related to regional terrain, weather, industrial production levels, and human activities.

According to the simulation evaluation results of five meteorological elements, the MB values between the simulated and observed values of temperature were between −2.1 °C and 1.43 °C, with a correlation coefficient greater than 0.85. The relative humidity was generally low, with an MB value of −24.52% to 3.79%, and the correlation coefficient was greater than 0.78. The simulation results of wind speeds showed that the MB in Xinyang was −2.63 m/s, and the values of other cities were between 0 and 0.56 m/s. For the correlation coefficient, except Jinan and Xinyang, which it was 0.59 and 0.65, all other cities had values greater than 0.78. The simulation results of wind speed showed that the R values in Jinan, Zhengzhou, Luoyang, and Xinyang were all greater than 0.5, while those of the other cities ranged from 0.31 to 0.48. A study has pointed out that poor simulation of ground wind direction by current meteorological models is a common problem [74]. It is particularly difficult to directly compare simulated meteorological values with observed values. Before the New Year's Day holiday (the cleaning period), the simulated values of Case17 had relatively consistent spatiotemporal distribution trends with the observed values. During and after the New Year's Day holiday (when pollution began to appear and worsened), Case16 accurately captured the regional high PM$_{2.5}$ concentrations, while Case17 underestimated it by more than 100 µg/m^3. From the simulation results, it is reasonable to use the difference between Case16 and Case17 to reflect the increases in PM$_{2.5}$ caused by human activities. In summary, the WRF-CMAQ model was able to reasonably simulate the meteorological and pollutant concentrations in this study.

Although the peaks of PM$_{2.5}$ increases caused by human activities varied in different regions, with those in some areas occurring during the holiday (Henan, Hubei, Hebei, and Anhui), and those in some cities appeared after the holiday (Zhengzhou, Luoyang, Xinyang, Jiaozuo, Luohe, Xiangyang, Jingzhou, Liaocheng, and Heze), there was no doubt that human activities led to increases in PM$_{2.5}$ concentrations during the holiday. For example, during the New Year's Day holiday in 2022, PM$_{2.5}$ levels in BTHS, YRD, central China, Hebei, Shandong, and Jiangsu increased by 36~96.25 µg/m^3. In addition, individual

cities (Jinan, Taiyuan, Zhengzhou, Luoyang, Nanyang, Xinyang, Jiaozuo, Luohe, Liaocheng, and Heze) had their PM$_{2.5}$ concentration increment valleys on 2 January, all of which were below 10 μg/m^3. The above results indicate that human activities had significant impacts on the New Year's Day effects of PM$_{2.5}$.

Before the New Year's Day holiday in 2022, the wind speed was relatively high, which was conducive to the diffusion of PM$_{2.5}$. During the New Year holiday, under the influence of westerly and northwest winds, areas with PM$_{2.5}$ expression in the Hebei, Shaanxi, and Henan provinces moved eastward. Subsequently, a cold air mass approached, coupled with sparse isobars, the wind speed decreased, and PM$_{2.5}$ continued to accumulate. After the holiday, the north wind played a dominant role, and pollution in the northern region was alleviated, while pollution in central China intensified, indicating that wind speed affected the transportation and accumulation of PM$_{2.5}$ between different regions. Observational data showed that when the ground temperature was low, the wind speed weakened, the air pressure decreased, and the humidity was high. As such, this condition was beneficial for the formation of air pollutions. Based on weather and meteorological analyses, when haze weather was accompanied by cloudy days or weak precipitation, the accumulation of water vapor and atmospheric aerosol pollutants near the ground would exacerbate the growth of PM, and there was a high possibility of heavy pollution. This result is consistent with the study of Cai et al. [75] and You et al. [76].

The industry source analysis in this study can to some extent explain the New Year's effects of PM$_{2.5}$. Before and after the New Year holiday, industrial production proceeded normally, and industrial sources made significant contributions to the formation of PM$_{2.5}$ (15~20 μg/m^3). During the New Year holiday, some factories shut down, and the contribution of industrial sources decreased (12~17 μg/m^3). However, this did not explain why the PM$_{2.5}$ concentrations during the holiday were higher than before. The analysis of changes in the contributions of transportation sources solved this problem. During the holiday, the contribution of transportation sources to PM$_{2.5}$ concentrations increased to 6~8 μg/m^3. This was likely due to frequent traffic activities and increased motor vehicle exhaust emissions during holidays for tourism and other purposes [77]. After the holiday, people took motor vehicles back to work, further leading to an increase in the contributions of transportation sources. However, the holiday effects during the Spring Festival period studied by Lei et al. [78] showed that PM$_{2.5}$ concentrations were higher during holiday than during non-holiday periods, which was different from the New Year's Day effects of PM$_{2.5}$ in this study. One important reason for this difference may be that in 2015, human factors such as setting off fireworks and firecrackers during the Spring Festival made a significant contribution to PM$_{2.5}$ concentrations. In 2022, the number of fireworks and firecrackers set off during the holiday decreased, resulting in a change in the holiday effect, and the peak PM$_{2.5}$ concentrations no longer appeared during the holiday period. Although the source of residential sources made the greatest contributions (60~100 μg/m^3) to PM$_{2.5}$, its contributions changed little during and around the holiday. Therefore, during and around the New Year's Day holiday, the main industry sources that caused changes in spatial and temporal distributions were industrial sources and transportation sources. The areas affected by these two emission sources expanded by 50% after the holiday compared to before and during the holiday.

However, the mutual influence between different regions during the pollution period is still unclear. PM$_{2.5}$ may spread from heavily polluted areas and affect the concentration of PM$_{2.5}$ in surrounding areas through regional transmission. In the future, ISAM tools can be used to quantitatively analyze the transmission of PM$_{2.5}$ between regions in order to propose specific regional joint prevention and control plans for PM$_{2.5}$ during and around the New Year's Day holiday.

5. Conclusions

This work studied the spatiotemporal variation characteristics of PM$_{2.5}$ during and around the New Year's Day holiday from 2015 to 2022 based on observational data. We

found that after 2019, the New Year's Day effects of PM$_{2.5}$ were significant, i.e., PM$_{2.5}$ concentrations showed a pattern of before the New Year's Day holiday < during the New Year's Day holiday < after the New Year's Day holiday. In order to explore the reasons for this phenomenon, this work used the WRF-CMAQ model to study the impacts of human activities on PM$_{2.5}$ concentrations during and before the New Year holiday in 2022, as well as the changes in contributions from different industry sources (residential, industrial, transportation, energy, and agricultural sources). The results indicate that frequent human activities during and after the holiday were the reasons for the significant New Year's Day effects of PM$_{2.5}$, and the contributions of industrial and transportation sources showed the greatest changes during and around the New Year holiday. This means that people's transportation activities during the New Year's Day holiday and the resumption of factory works after the holiday exacerbated PM$_{2.5}$ pollutions. These results can provide a valuable reference for the prevention of air pollution during and after holidays.

References

1. Shen, R.; Schäfer, K.; Shao, L.; Schnelle-Kreis, J.; Wang, Y.; Li, F.; Liu, Z.; Emeis, S.; Schmid, H.P. Chemical characteristics of PM$_{2.5}$ during haze episodes in spring 2013 in Beijing. *Urban CLim.* **2017**, *22*, 51–63. [CrossRef]
2. Huang, R.J.; Zhang, Y.; Bozzetti, C.; Ho, K.F.; Cao, J.J.; Han, Y.; Daellenbach, K.R.; Slowik, J.G.; Platt, S.M.; Canonaco, F.; et al. High secondary aerosol contribution to particulate pollution during haze events in China. *Nature* **2014**, *514*, 218–222. [CrossRef] [PubMed]
3. Lei, Y.; Zhang, Q.; He, K.B.; Streets, D.G. Primary anthropogenic aerosol emission trends for China, 1990–2005. *Atmos. Chem. Phys.* **2011**, *11*, 931–954. [CrossRef]
4. Querol, X.; Alastuey, A.; Rodriguez, S.; Plana, F.; Mantilla, E.; Ruiz, C.R. Monitoring of PM$_{10}$ and PM$_{2.5}$ around primary particulate anthropogenic emission sources. *Atmos. Environ.* **2001**, *35*, 845–858. [CrossRef]
5. Zheng, B.; Zhang, Q.; Zhang, Y.; He, K.B.; Wang, K.; Zheng, G.J.; Duan, F.K.; Ma, Y.L.; Kimoto, T. Heterogeneous chemistry: A mechanism missing in current models to explain secondary inorganic aerosol formation during the January 2013 haze episode in North China. *Atmos. Chem. Phys.* **2015**, *15*, 2031–2049. [CrossRef]
6. Janssens-Maenhout, G.; Crippa, M.; Guizzardi, D.; Dentener, F.; Muntean, M.; Pouliot, G.; Keating, T.; Zhang, Q.; Kurokawa, J.; Wankmüller, R.; et al. HTAP_v2.2: A mosaic of regional and global emission grid maps for 2008 and 2010 to study hemispheric transport of air pollution. *Atmos. Chem. Phys.* **2015**, *15*, 11411–11432. [CrossRef]
7. Guo, S.; Hu, M.; Zamora, M.L.; Peng, J.; Shang, D.; Zheng, J.; Du, Z.; Wu, Z.; Shao, M.; Zeng, L.; et al. Elucidating severe urban haze formation in China. *Proc. Natl. Acad. Sci. USA* **2014**, *111*, 17373–17378. [CrossRef] [PubMed]
8. Prospero, J.M. Long-term measurements of the transport of African mineral dust to the southeastern United States: Implications for regional air quality. *J. Geophys. Res.-Atmos.* **1999**, *104*, 15917–15927. [CrossRef]
9. Guelle, W.; Balkanski, Y.J.; Schulz, M.; Marticorena, B.; Bergametti, G.; Moulin, C.; Arimoto, R.; Perry, K.D. Modeling the atmospheric distribution of mineral aerosol: Comparison with ground measurements and satellite observations for yearly and synoptic timescales over the North Atlantic. *J. Geophys. Res.-Atmos.* **2000**, *105*, 1997–2012. [CrossRef]

10. Pinkerton, K.E.; Green, F.H.Y.; Saiki, C.; Vallyathan, V.; Plopper, C.G.; Gopal, V.; Hung, D.; Bahne, E.B.; Lin, S.S.; Ménache, M.G.; et al. Distribution of particulate matter and tissue remodeling in the human lung. *Environ. Health Perspect.* **2000**, *108*, 1063–1069. [CrossRef]

11. Xu, D.; Huang, N.; Wang, Q.; Liu, H. Study of ambient PM$_{2.5}$ on the influence of the inflammation injury and the immune function of subchronic exposure rats. *J. Hyg. Res.* **2008**, *37*, 423–428.

12. Wang, G.; Jiang, R.; Zhao, Z.; Song, W. Effects of ozone and fine particulate matter (PM$_{2.5}$) on rat system inflammation and cardiac function. *Toxicol. Lett.* **2013**, *217*, 23–33. [CrossRef] [PubMed]

13. Hu, Z. Spatial analysis of MODIS aerosol optical depth, PM$_{2.5}$, and chronic coronary heart disease. *Int. J. Health Geogr.* **2009**, *8*, 27. [CrossRef] [PubMed]

14. Madrigano, J.; Kloog, I.; Goldberg, R.; Coull, B.A.; Mittleman, M.A.; Schwartz, J. Long-term exposure to PM$_{2.5}$ and incidence of acute myocardial infarction. *Environ. Health Perspect.* **2013**, *121*, 192–196. [CrossRef] [PubMed]

15. Barrett, J.R. Apples to Apples: Comparing PM$_{2.5}$ exposures and birth outcomes in understudied countries. *Environ. Health Perspect.* **2014**, *122*, A110. [CrossRef] [PubMed]

16. Watterson, T.L.; Sorensen, J.; Martin, R.; Coulombe, R.A., Jr. Effects of PM$_{2.5}$ collected from Cache Valley Utah on genes associated with the inflammatory response in human lung cells. *J. Toxicol. Environ. Health Part A* **2007**, *70*, 1731–1744. [CrossRef] [PubMed]

17. Chen, H.; Burnett, R.T.; Kwong, J.C.; Villeneuve, P.J.; Goldberg, M.S.; Brook, R.D.; van Donkelaar, A.; Jerrett, M.; Martin, R.V.; Brook, J.R.; et al. Risk of incident diabetes in relation to long-term exposure to fine particulate matter in Ontario, Canada. *Environ. Health Perspect.* **2013**, *121*, 804–810. [CrossRef] [PubMed]

18. Zanobetti, A.; Dominici, F.; Wang, Y.; Schwartz, J.D. A national case-crossover analysis of the short-term effect of PM$_{2.5}$ on hospitalizations and mortality in subjects with diabetes and neurological disorders. *Environ. Health* **2014**, *13*, 11. [CrossRef]

19. Franklin, M.; Zeka, A.; Schwartz, J. Association between PM$_{2.5}$ and all-cause and specific-cause mortality in 27 US communities. *J. Expo. Sci. Environ. Epidemiol.* **2007**, *17*, 279–287. [CrossRef]

20. Fann, N.; Lamson, A.D.; Anenberg, S.C.; Wesson, K.; Risley, D.; Hubbell, B.J. Estimating the national public health burden associated with exposure to ambient PM$_{2.5}$ and ozone. *Risk Anal.* **2012**, *32*, 81–95. [CrossRef]

21. Elliott, C.T.; Copes, R. Burden of mortality due to ambient fine particulate air pollution (PM$_{2.5}$) in interior and northern BC. *Can. J. Public Health-Rev. Can. Sante Publ.* **2011**, *102*, 390–393. [CrossRef] [PubMed]

22. Xu, L.; Batterman, S.; Chen, F.; Li, J.; Zhong, X.; Feng, Y.; Rao, Q.; Chen, F. Spatiotemporal characteristics of PM$_{2.5}$ and PM$_{10}$ at urban and corresponding background sites in 23 cities in China. *Sci. Total Environ.* **2017**, *599–600*, 2074–2084. [CrossRef] [PubMed]

23. Zhou, C.; Chen, J.; Wang, S. Examining the effects of socioeconomic development on fine particulate matter (PM$_{2.5}$) in China's cities using spatial regression and the geographical detector technique. *Sci. Total Environ.* **2018**, *619–620*, 436–445. [CrossRef] [PubMed]

24. Li, R.; Wang, Z.; Cui, L.; Fu, H.; Zhang, L.; Kong, L.; Chen, W.; Chen, J. Air pollution characteristics in China during 2015-2016: Spatiotemporal variations and key meteorological factors. *Sci. Total Environ.* **2019**, *648*, 902–915. [CrossRef] [PubMed]

25. Dai, F.; Chen, M.; Yang, B. Spatiotemporal variations of PM$_{2.5}$ concentration at the neighborhood level in five Chinese megacities. *Atmos. Pollut. Res.* **2020**, *11*, 190–202. [CrossRef]

26. Song, C.; Wu, L.; Xie, Y.; He, J.; Chen, X.; Wang, T.; Lin, Y.; Jin, T.; Wang, A.; Liu, Y.; et al. Air pollution in China: Status and spatiotemporal variations. *Environ. Pollut.* **2017**, *227*, 334–347. [CrossRef]

27. Wei, J.; Li, Z.; Lyapustin, A.; Sun, L.; Peng, Y.; Xue, W.; Su, T.; Cribb, M. Reconstructing 1-km-resolution high-quality PM$_{2.5}$ data records from 2000 to 2018 in China: Spatiotemporal variations and policy implications. *Remote Sens. Environ.* **2021**, *252*, 112136. [CrossRef]

28. Guo, B.; Wang, X.; Pei, L.; Su, Y.; Zhang, D.; Wang, Y. Identifying the spatiotemporal dynamic of PM$_{2.5}$ concentrations at multiple scales using geographically and temporally weighted regression model across China during 2015–2018. *Sci. Total Environ.* **2021**, *751*, 141765. [CrossRef] [PubMed]

29. Wang, S.; Zhou, C.; Wang, Z.; Feng, K.; Hubacek, K. The characteristics and drivers of fine particulate matter (PM$_{2.5}$) distribution in China. *J. Clean. Prod.* **2017**, *142*, 1800–1809. [CrossRef]

30. Deng, X.; Zeng, X. Spatial and temporal analysis of the Spring Festival effect on air pollutants in 31 cities of China. *J. Ear. Environ.* **2021**, *12*, 159–169.

31. Chang, J.L.; Yu, H.; Luo, W.W.; Wang, L. Holiday Effect of Spring Festival on PM$_{2.5}$ Pollution in Chang-Zhu-Tan Metropolitan Area. *J. Ecol. Rural Environ.* **2016**, *32*, 724–728. [CrossRef]

32. Zhou, J.-b.; Duan, J.C.; Wang, J.G.; Yang, P.; Liu, H.W.; Li, M.; Jin, W. Analysis of pollution characteristics and sources of PM$_{2.5}$ during heavy pollution in Shijiazhuang City around New Year's Day 2019. *Chin. J. Environ. Sci.* **2020**, *41*, 39–49. [CrossRef]

33. Skamarock, W.C.; Klemp, J.B.; Dudhia, J.; Gill, D.O.; Barker, D.; Duda, M.G.; Powers, J.G. A description of the Advanced Research WRF Version 3 (No. NCAR/TN-475+STR). *Univ. Corp. Atmos. Res.* **2008**, *1*, 1. [CrossRef]

34. Gochis, D.J.; Coen, J.L.; Gill, D.O.; Dudhia, J.; Davis, C.A.; Skamarock, W.C.; Klemp, J.B.; Powers, J.G.; Ahmadov, R.; Peckham, S.E.; et al. The Weather Research and Forecasting Model: Overview, system efforts, and future directions. *Bull. Amer. Meteorol. Soc.* **2017**, *98*, 1717–1737. [CrossRef]

35. Shikhovtsev, A.Y.; Kovadlo, P.G.; Lezhenin, A.A.; Korobov, O.A.; Kiselev, A.V.; Russkikh, I.V.; Kolobov, D.Y.; Shikhovtsev, M.Y. Influence of atmospheric flow structure on optical turbulence characteristics. *Appl. Sci.* **2023**, *13*, 1282. [CrossRef]

36. Castorina, G.; Semprebello, A.; Insinga, V.; Italiano, F.; Caccamo, M.T.; Magazù, S.; Morichetti, M.; Rizza, U. Performance of the WRF model for the Forecasting of the V-shaped storm recorded on 11–12 November 2019 in the eastern Sicily. *Atmosphere* **2023**, *14*, 390. [CrossRef]

37. Byun, D.; Schere, K.L. Review of the governing equations, computational algorithms, and other components of the models-3 Community Multiscale Air Quality (CMAQ) modeling system. *Appl. Mech. Rev.* **2006**, *59*, 51–77. [CrossRef]

38. Gao, Z.; Zhou, X. A review of the CAMx, CMAQ, WRF-Chem and NAQPMS models: Application, evaluation and uncertainty factors. *Environ. Pollut.* **2024**, *343*, 123183. [CrossRef] [PubMed]

39. Zhang, Y.; Chen, X.; Yu, S.; Wang, L.; Li, Z.; Li, M.; Liu, W.; Li, P.; Rosenfeld, D.; Seinfeld, J.H. City-level air quality improvement in the Beijing-Tianjin-Hebei region from 2016/17 to 2017/18 heating seasons: Attributions and process analysis. *Environ. Pollut.* **2021**, *274*, 116523. [CrossRef]

40. Jiang, Y.; Yu, S.; Chen, X.; Zhang, Y.; Li, M.; Li, Z.; Song, Z.; Li, P.; Zhang, X.; Lichtfouse, E.; et al. Large contributions of emission reductions and meteorological conditions to the abatement of $PM_{2.5}$ in Beijing during the 24th Winter Olympic Games in 2022. *J. Environ. Sci.* **2024**, *136*, 172–188. [CrossRef]

41. Ge, Y.Z.; Chen, C.Q.; Jiang, Y.P.; Yang, T.S.; Kang, H.Y.; Li, J.Z.; Zhao, X.R.; Zhang, Y.B.; Li, M.Y.; Hou, T.Y.; et al. Characteristics of ozone pollution in tai'an and topographic effects of Mount Tai. *Atmosphere* **2022**, *13*, 1299. [CrossRef]

42. Im, U.; Markakis, K.; Unal, A.; Kindap, T.; Poupkou, A.; Incecik, S.; Yenigun, O.; Melas, D.; Theodosi, C.; Mihalopoulos, N. Study of a winter PM episode in Istanbul using the high resolution WRF/CMAQ modeling system. *Atmos. Environ.* **2010**, *44*, 3085–3094. [CrossRef]

43. Wang, J.; Shi, W.H.; Xue, K.X.; Wu, T.; Fang, C.S. Analysis of the impact of meteorological factors on ambient air quality during the COVID-19 lockdown in Jilin City in 2022. *Atmosphere* **2023**, *14*, 400. [CrossRef]

44. Hogrefe, C.; Pouliot, G.; Wong, D.; Torian, A.; Roselle, S.; Pleim, J.; Mathur, R. Annual application and evaluation of the online coupled WRF-CMAQ system over North America under AQMEII phase 2. *Atmos. Environ.* **2015**, *115*, 683–694. [CrossRef]

45. Feng, R.; Wang, Q.; Huang, C.C.; Liang, J.; Luo, K.; Fan, J.R.; Cen, K.F. Investigation on air pollution control strategy in Hangzhou for post-G20/pre-Asian-games period (2018–2020). *Atmos. Pollut. Res.* **2019**, *10*, 197–208. [CrossRef]

46. Mazzeo, A.; Zhong, J.; Hood, C.; Smith, S.; Stocker, J.; Cai, X.M.; Bloss, W.J. Modelling the impact of national vs. local emission reduction on $PM_{2.5}$ in the West Midlands, UK using WRF-CMAQ. *Atmosphere* **2022**, *13*, 377. [CrossRef]

47. Wang, L.; Chen, X.; Zhang, Y.; Li, M.; Li, P.; Jiang, L.; Xia, Y.; Li, Z.; Li, J.; Wang, L.; et al. Switching to electric vehicles can lead to significant reductions of $PM_{2.5}$ and NO_2 across China. *One Earth* **2021**, *4*, 1037–1048. [CrossRef]

48. Deng, T.; Chen, Y.; Wan, Q.L.; Zhang, Y.X.; Deng, X.J.; Huang, Y.Y.; Dai, G.F.; Li, F. Comparative evaluation of the impact of GRAPES and MM5 meteorology on CMAQ prediction over Pearl River Delta, China. *Particuology* **2018**, *40*, 88–97. [CrossRef]

49. Djalalova, I.; Delle Monache, L.; Wilczak, J. $PM_{2.5}$ analog forecast and Kalman filter post-processing for the Community Multiscale Air Quality (CMAQ) model. *Atmos. Environ.* **2015**, *108*, 76–87. [CrossRef]

50. Wang, N.; Guo, H.; Jiang, F.; Ling, Z.H.; Wang, T. Simulation of ozone formation at different elevations in mountainous area of Hong Kong using WRF-CMAQ model. *Sci. Total Environ.* **2015**, *505*, 939–951. [CrossRef]

51. Hu, J.L.; Chen, J.J.; Ying, Q.; Zhang, H.L. One-year simulation of ozone and particulate matter in China using WRF/CMAQ modeling system. *Atmos. Chem. Phys.* **2016**, *16*, 10333–10350. [CrossRef]

52. Hong, C.P.; Zhang, Q.; Zhang, Y.; Tang, Y.H.; Tong, D.; He, K.B. Multi-year downscaling application of two-way coupled WRF v3.4 and CMAQ v5.0.2 over east Asia for regional climate and air quality modeling: Model evaluation and aerosol direct effects. *Geosci. Model Dev.* **2017**, *10*, 2447–2470. [CrossRef]

53. Vemuri, A.; Buckingham, S.; Munters, W.; Helsen, J.; van Beeck, J. Sensitivity analysis of mesoscale simulations to physics parameterizations over the Belgian North Sea using Weather Research and Forecasting—Advanced Research WRF (WRF-ARW). *Wind Energy Sci.* **2022**, *7*, 1869–1888. [CrossRef]

54. Wang, L.; Yu, S.; Li, P.; Chen, X.; Li, Z.; Zhang, Y.; Li, M.; Mehmood, K.; Liu, W.; Chai, T.; et al. Significant wintertime $PM_{2.5}$ mitigation in the Yangtze River Delta, China, from 2016 to 2019: Observational constraints on anthropogenic emission controls. *Atmos. Chem. Phys.* **2020**, *20*, 14787–14800. [CrossRef]

55. Li, P.; Wang, L.; Guo, P.; Yu, S.; Mehmood, K.; Wang, S.; Liu, W.; Seinfeld, J.H.; Zhang, Y.; Wong, D.C.; et al. High reduction of ozone and particulate matter during the 2016 G-20 summit in Hangzhou by forced emission controls of industry and traffic. *Environ. Chem. Lett.* **2017**, *15*, 709–715. [CrossRef] [PubMed]

56. Wu, Y.; Wang, P.; Yu, S.; Wang, L.; Li, P.; Li, Z.; Mehmood, K.; Liu, W.; Wu, J.; Lichtfouse, E.; et al. Residential emissions predicted as a major source of fine particulate matter in winter over the Yangtze River Delta, China. *Environ. Chem. Lett.* **2018**, *16*, 1117–1127. [CrossRef]

57. Yu, S.; Mathur, R.; Pleim, J.; Wong, D.; Gilliam, R.; Alapaty, K.; Zhao, C.; Liu, X. Aerosol indirect effect on the grid-scale clouds in the two-way coupled WRF–CMAQ: Model description, development, evaluation and regional analysis. *Atmos. Chem. Phys.* **2014**, *14*, 11247–11285. [CrossRef]

58. Gasparini, B.; Meyer, A.; Neubauer, D.; Münch, S.; Lohmann, U. Cirrus cloud properties as seen by the *CALIPSO* satellite and ECHAM-HAM global climate model. *J. Clim.* **2018**, *31*, 1983–2003. [CrossRef]

59. Xiu, A.J.; Pleim, J.E. Development of a land surface model. Part I: Application in a mesoscale meteorological model. *J. Appl. Meteorol.* **2001**, *40*, 192–209. [CrossRef]

60. Pleim, J.E. A combined local and nonlocal closure model for the atmospheric boundary layer. Part I: Model description and testing. *J. Appl. Meteorol. Climatol.* **2007**, *46*, 1383–1395. [CrossRef]
61. Pleim, J.E. A combined local and nonlocal closure model for the atmospheric boundary layer. Part II: Application and evaluation in a mesoscale meteorological model. *J. Appl. Meteorol. Climatol.* **2007**, *46*, 1396–1409. [CrossRef]
62. Morrison, H.; Curry, J.A.; Khvorostyanov, V.I. A new double-moment microphysics parameterization for application in cloud and climate models. Part I: Description. *J. Atmos. Sci.* **2005**, *62*, 1665–1677. [CrossRef]
63. Morrison, H.; Pinto, J.O. Intercomparison of bulk cloud microphysics schemes in mesoscale simulations of springtime Arctic mixed-phase stratiform clouds. *Mon. Weather Rev.* **2006**, *134*, 1880–1900. [CrossRef]
64. Kain, J.S. The Kain-Fritsch convective parameterization: An update. *J. Appl. Meteorol.* **2004**, *43*, 170–181. [CrossRef]
65. Li, M.; Zhang, Q.; Kurokawa, J.; Woo, J.H.; He, K.B.; Lu, Z.F.; Ohara, T.; Song, Y.; Streets, D.G.; Carmichael, G.R.; et al. MIX: A mosaic Asian anthropogenic emission inventory under the international collaboration framework of the MICS-Asia and HTAP. *Atmos. Chem. Phys.* **2017**, *17*, 935–963. [CrossRef]
66. Kwok, R.H.F.; Napelenok, S.L.; Baker, K.R. Implementation and evaluation of $PM_{2.5}$ source contribution analysis in a photochemical model. *Atmos. Environ.* **2013**, *80*, 398–407. [CrossRef]
67. Mishra, P.; Singh, U.; Pandey, C.M.; Mishra, P.; Pandey, G. Application of student's t-test, analysis of variance, and covariance. *Ann. Card. Anaesth.* **2019**, *22*, 407–411. [CrossRef]
68. Mao, W.; Xu, J.; Lu, D.; Yang, D.; Zhao, J. An analysis of the spatial-temporal pattern and influencing fctors of $PM_{2.5}$ in the Yangtze River Delta in 2015. *Resour. Environ. Yangtze Val.* **2017**, *26*, 264–272.
69. Yu, S.C.; Eder, B.; Dennis, R.; Chu, S.H. New unbiased symmetricmetrics for evaluation of air quality models. *Atmos. Sci. Lett.* **2006**, *7*, 26–34. [CrossRef]
70. Emery, C.; Liu, Z.; Russell, A.G.; Odman, M.T.; Yarwood, G.; Kumar, N. Recommendations on statistics and benchmarks to assess photochemical model performance. *J. Air Waste Manag. Assoc.* **2017**, *67*, 582–598. [CrossRef]
71. Feng, S.Z.; Jiang, F.; Wang, H.M.; Shen, Y.; Zheng, Y.H.; Zhang, L.Y.; Lou, C.X.; Ju, W.M. Anthropogenic emissions estimated using surface observations and their impacts on $PM_{2.5}$ source apportionment over the Yangtze River Delta, China. *Sci. Total Environ.* **2022**, *828*, 13. [CrossRef] [PubMed]
72. Feng, Y.; Ning, M.; Lei, Y.; Sun, Y.; Liu, W.; Wang, J. Defending blue sky in China: Effectiveness of the "Air Pollution Prevention and Control Action Plan" on air quality improvements from 2013 to 2017. *J. Environ. Manag.* **2019**, *252*, 109603. [CrossRef] [PubMed]
73. Zeng, Y.; Cao, Y.; Qiao, X.; Seyler, B.C.; Tang, Y. Air pollution reduction in China: Recent success but great challenge for the future. *Sci. Total Environ.* **2019**, *663*, 329–337. [CrossRef] [PubMed]
74. Bai, C.; Yan, P. Dependence analysis of $PM_{2.5}$ concentrations in 295 Chinese cities in the winter of 2019–2020. *Atmosphere* **2022**, *13*, 1847. [CrossRef]
75. Cai, Z.; Jiang, F.; Chen, J.M.; Jiang, Z.Q.; Wang, X.Y. Weather condition dominates regional $PM_{2.5}$ Pollutions in the eastern coastal provinces of China during winter. *Aerosol. Air Qual. Res.* **2018**, *18*, 969–980. [CrossRef]
76. You, T.; Wu, R.G.; Huang, G.; Fan, G.Z. Regional meteorological patterns for heavy pollution events in Beijing. *J. Meteorol. Res.* **2017**, *31*, 597–611. [CrossRef]
77. Huang, Q.; Zeng, F.; Xiao, H.; Zeng, Z.; Sun, Q. Stable isotopic compositions of carbon and nitrogen in aerosol samples collected from the Pingxiang City and their source apportionment. *Bull. Miner. Petrol. Geochem.* **2019**, *38*, 114–120.
78. Lei, Y.; Zhang, X.; Tang, Y.; Fan, G.; Zhou, D. Holiday effects on $PM_{2.5}$ and other major pollutants in Beijing. *Acta Sci. Circumstantiae* **2015**, *35*, 1520–1528.